A multi-scale model analysis of ozone formation in the Bangkok Metropolitan Region, Thailand

Pornpan Uttamang[1,2], Patrick C. Campbell[3], Viney P. Aneja[1] and Adel F. Hanna[4]

[1]Department of Marine, Earth, and Atmospheric Sciences, North Carolina State University, Raleigh, NC, 27695, USA.
[2](now at) Faculty of Science, Maejo University, Chiang Mai, 50290, Thailand.
[3]Cooperative Institute for Satellite Earth System Studies (CISESS), George Mason University, NOAA Air Resources Laboratory Affiliate, College Park, MD, 20740, USA.
[4]Institute for the Environment, University of North Carolina at Chapel Hill, Chapel Hill, NC, 27517, USA.

Correspondence to: Pornpan Uttamang (puttama@ncsu.edu)

Abstract

Over the last three decades, Thailand's rapid industrialization and urbanization have led to an impact on urban air quality. A majority of the country's development has occurred within and around Bangkok (BKK), the capital city of Thailand, and the Bangkok Metropolitan Region (BMR). Since 1995, the BMR has experienced air quality degradation, in particular, enhanced ozone (O_3) due to a combination of the local increase in emissions from accelerated growth in automotive and industrial activities, local meteorology including strong solar radiation, high temperature and high humidity, and potential long-range effects of regional transport from China. To investigate the O_3 formation in the BMR due to the effects of long-range transport and local meteorology feedbacks, we perform a multi-scale simulation with the Weather Research and Forecasting model with Chemistry (WRF-Chem) during the O_3 season (January to March), 2010; since O_3 mixing ratio exceedances in the BMR occur primarily during this period The results in this study indicate the significance of China's emission reductions on the regional-scale and the local-scale pollutions, as far as the BMR region and southern Thailand. Applying China's oxide of nitrogen (NO_x)-only emission controls, generally, enhance the domain-wide monthly-average peroxyacetyl nitrate (PAN) and O_3 in the regional scale, in the order of ~1 to 7% and ~1 to 5%, respectively, while those in the local scale are ~ 0.2 to 6% and ~0.1 to 5% compared with the baseline simulation. However, the increases in PAN and O_3 are mitigated by 40% China's Volatile Organic Compound (VOC) reduction along with 40% NO_x reduction. The results, supported by an indicator analysis, suggest that northern and eastern China, northern and central Thailand and the BMR, are likely VOC-limited during the O_3 season. Since the BMR is VOC-limited regime, controlling anthropogenic VOC emissions will show more benefit to control O_3 than controlling NO_x-only emissions. Other factors that influence on O_3 levels in the BMR are biogenic VOC emissions from the Tenasserim range and land- and sea-breeze circulations that recirculate and disperse pollutants along the coastal areas.

Keywords: Long-range transport; Surface ozone; WRF-Chem; VOC-limited; NO_x-limited

1. Introduction

The Bangkok Metropolitan Region (BMR) has experienced air quality degradation over the past few decades, due to rapid economic growth, and an increase in pollutant emissions (Bucher et al., 2011; Chueinta et al., 2000; Oanh et al., 2006; Oanh and Zhang, 2004; Ruchirawat et al., 2002; Uttamang et al., 2018). These enhanced emissions are harmful to human health, and the environment (Bucher et al., 2011; Oanh et al., 2006; Ruchirawat et al., 2002; Uttamang et al., 2018). Pollution Control Department (PCD), Thailand (2012) reported that, in Thailand, annual average mixing ratios of O_3 during 2005 to 2012 (17 years) had been increasing continuously due to long-range transport and increases in volatile organic compounds (VOC) emissions. During 2012, more than 80 % of the monitoring stations located in Thailand reported exceeded O_3 mixing ratios which very high mixing ratios of O_3 were observed in Bangkok and its vicinities (PCD, 2012). Our previous study on air quality in the BMR (Uttamang et al., 2018) showed that during 2010 to 2014, among other gaseous criteria pollutants, ozone (O_3) was the only gaseous species whose mixing ratios frequently exceeded Thailand National Ambient Air Quality standard (NAAQs) for O_3 (Thailand NAAQs for hourly O_3 is 100 ppb [PCD, 2018]). Moreover, the annual average O_3 mixing ratios had been increasing during 2010 to 2014 (~16.5 ppb in 2010 and ~20.0 ppb in 2014). The hourly O_3 exceedances in the BMR were frequently observed during the dry season (local summer starts from February to May and local winter starts from October to February), especially in January to March when Northeast monsoon winds were the predominant wind direction. Those values were less observed during the transitional period between wet and dry seasons (i.e. during May) and rarely occurred during wet season (May to October) (Uttamang et al., 2018). Annual average mixing ratios of CO, SO_2, O_3 and NO_2 during 2003 to 2014 in the BMR are shown in table S1, supplement material.

East Asia's pollutant emissions play an important role in regional and global air quality. In 2010, emissions of oxide of nitrogen (NO_x = NO + NO_2), sulfur dioxide (SO_2), coarse mode particulate matter (PM_{10}), fine mode particulate matter ($PM_{2.5}$), and non-methane volatile organic compounds (NMVOC) over East Asia were 29.7 Mt, 29.5 Mt, 16.8 Mt, 12.5 Mt, and 25.9 Mt, respectively (Wang et al., 2014b). Compared to the total emissions in East Asia, China contributes ~ 82 to 88 % of NO_x, ~ 94 % of SO_2 and ~ 84 to 88 % of PM_{10} and $PM_{2.5}$ (Wang et al., 2014b). Several emission control strategies have been suggested to reduce current and future pollution in China (Guo et al., 2014; Liang et al., 2017; Shao et al., 2009; Sun et al., 2018; Xue et al., 2014); however, the reduction targets for major air pollutants are not clear (Zhang et al., 2017, 2014). A 10% NO_x emission reduction from 2010 levels was proposed as the national reduction target during China's 12th Five Year Plan (FYP) (2011 to 2015) (Wang et al., 2014a). By applying this strategy, the hourly maximum O_3 mixing ratios in China were reduced ~ 2 % (Wang et al., 2014a). Different emission control strategies were proposed in Shanghai, Jiangsu and Zhejiang. The proposed anthropogenic NO_x emission reductions during the 12th FYP were by 17.5 %, 17.5 % and 18 %, respectively (Zhang et al., 2017). According to the ambient air quality guidelines set by the World Health Organization (WHO), China needs to reduce 60 % of SO_2 emissions along with 40 % of NO_x and volatile organic compounds (VOC), and 50 % of PM_{10} emissions from 2005, in order to attain the guidelines (Wang and Hao, 2012).

The effects of long-range transport of air pollutants originating in China on ambient air

pollution in Asian countries have been reported in several studies. Kim et al. (2009) reported that the increases in PM_{10}, $PM_{2.5}$ and ionic components of particulate matters over a remote area in Hong Kong was influenced by air masses originating from northern and eastern China. Lee et al. (2013) and Oh et al. (2015) reported that high PM_{10} levels over Seoul, Korea were caused, in part, from a combination of transboundary pollutants from northern and eastern China and local meteorology (high-pressure system and atmospheric circulation) over Korea. Cuesta et al. (2018) reported that O_3 pollution plumes transported by an anticyclonic circulation from the North China Plain to northern China, Korea and Japan, resulted in elevated O_3 levels over Japan.

In this paper, we examined O_3 behavior and regional processes that contribute to elevated O_3 levels in the BMR; in particular, the role of NO_x and VOC emissions in China and the subsequent transport of trace gases and aerosols to the BMR as elevated O_3 mixing ratios are frequently observed during dry seasons when there is a predominant Northeast monsoon wind direction. The effect of China's emission control strategies on O_3 levels in the BMR was investigated using the Weather Research and Forecasting model version 3.9.1 coupled with chemistry (WRF-Chem). We first evaluated the performance of the WRF model to simulate meteorology and O_3 mixing ratios in the BMR. Then we examined the impacts of NO_x and VOCs emission reductions in China on transboundary O_3 precursors transport, and the resulting effect on O_3 levels in the BMR region.

2. Model configuration and simulation design

2.1 WRF-Chem model configuration

WRF-Chem is a fully coupled online chemical and meteorological model (Grell et al., 2005), which has been widely used for regional-scale air quality studies (Guo et al., 2016; Jose et al., 2017; Karagulian et al., 2019; Liua et al., 2016; Podrascanin, 2019; Sharma et al., 2017; Tessum et al., 2015; Thompson et al., 2008; Yahya et al., 2017).

Figure 1 illustrates a triple-nested domain using in this study and 36- (the outermost domain [d01]), 12- (the second domain [d02]) and 4-km (the innermost domain [d03]) horizontal resolutions, which results in 98 × 150, 88 × 106 and 97 × 97 east-west and north-south grid points, respectively. The model vertical resolution consists of 33 sigma-pressure vertical layers. D01 covers Thailand and most part of the region of China, where d02 and d03 scale down to the region of Thailand and the BMR, respectively.

Table 1 summarizes the physics and chemistry options used in this study. Here we use the Thompson scheme for grid-scale microphysics (Thompson et al., 2008), the Grell-Freitas cumulus parameterization (Grell and Freitas, 2014), the Rapid Radiative Transfer Model (RRTMG) for the longwave and shortwave radiation (Iacono et al., 2008), the Yonsei University planetary boundary layer (YSU-PBL) scheme (Hong et al., 2006), the MM5 similarity surface layer scheme (Fairall et al., 2003), and the Noah Land-Surface model (Noah-LSM) (Chen and Dudhia, 2001) with the united States Geological Survey (USGS) landuse dataset.

The Regional Acid Deposition Model version 2 (RADM2) couples with Model Aerosol Dynamics Model for Europe/Secondary Organic Aerosol Model (MADE/SORGAM) is used to simulate the gas-phase mechanism, and aerosol physics and chemistry, respectively. The RADM2

is one of the most computationally efficient mechanisms to calculate O_3 and photochemical reactions of gaseous species (Zimmermann and Poppe, 1996). Three particle modes (Aitken, accumulation and coarse mode) and three major particle dynamics (nucleation, condensational growth and coagulation) are simulated using the MADE/SORGRAM aerosol module by assuming the particle size distribution is log-normal (Yang et al., 2018). The Madronich F-TUV is selected for photolysis scheme. The chemistry is configured to run with dry deposition of gas species and aerosols, subgrid convective wet scavenging and aqueous chemistry, vertical turbulent mixing, and direct and indirect feedbacks from the aerosols to the radiation schemes.

The total simulation period is 18 December 2009 to 31 March 2010 (which includes an O_3 episode which occurred during 5 to 6 March 2010). The first two weeks (18 to 31 December 2010) used as model spin-up (excluded from model analysis), and a 10-day meteorological re-initialization strategy with continuous chemistry.

2.2 Input data

The meteorological simulation is driven by the National Centers for Environmental Prediction-Final Operational Global Analysis data (NCEP-FNL) with $1^\circ \times 1^\circ$ spatial resolution prepared operationally every six hours. Amnuaylojaroen et al. (2014) studied the effects of different emission inventories including the Reanalysis of the TROpospheric chemical composition (RETRO), the Intercontinental Chemical Transport Experiment-Phase B (INTEX-B), the MACCity emissions (adapted from the Monitoring Atmospheric Composition and Climate and megacity Zoom for the Environment projects), the Southeast Asia Composition, Cloud, Climate Coupling Regional Study (SEAC4RS) emissions, and a combination of MACCity and SEAC4RS emissions on simulated O_3 by using WRF-Chem in Southeast Asia. Their results showed that the difference among those emission inventories might reach ~ 30%, and the WRF-Chem model generated only a slight variability of O_3 mixing ratios (~8 %). Lamarque et al. (2010) reported that the global total amount of anthropogenic emissions from RETRO was similar to those from the Emissions Database for Global Atmospheric Research emission inventory (EDGAR), eventhough specific sectors or regions in those inventories were different.

In this study, monthly average Emissions Database for Global Atmospheric Research-Hemispheric Transport of Air Pollution (EDGAR-HTAP) for the year 2010 with the finest horizontal resolution ($0.1^\circ \times 0.1^\circ$ spatial resolution) is selected (Janssens-Maenhout et al., 2012) (http://edgar.jrc.ec.europa.eu/htap_v2/). This inventory contains CO, NO_x, SO_2, NMVOC, ammonia (NH_3), methane (CH_4), PM_{10}, $PM_{2.5}$, organic compound (OC) and black carbon (BC) emissions from power, industrial, residential, agriculture, and transport (ground, air and shipping) sectors. The EDGAR-HTAP emissions were spatially processed for the specific trace gas and aerosol emission species needed for RADM2-MADE/SORGAM using the PREP-CHEM-Sources preprocessor, version 1.5 (Oliveira et al., 2016), and then were subsequently processed to be model-ready using the WRF-Chem "convert_emiss" program. Biogenic emissions data are calculated inline in WRF-Chem using the Model of Emissions of Gases and Aerosols from Nature version 2 (MEGAN) (Guenther et al., 2006).

Chemical initial and boundary conditions (ICs/BCs) are prepared using the Model for Ozone and Related Chemical Tracers, version 4, which is driven by meteorological fields from the

Goddard Earth Observing System Model, Version 5 (MOZART-4/GEOS-5) with 1.9 ° × 2.5° horizontal resolution, and 56 vertical layers (Emmons et al., 2010).

2.3 Simulation design

A baseline simulation is set following the model configurations in section 2.1. The results from the baseline simulation are used for model evaluation. Long-range transport of O_3 and its precursors (NO_x and VOC) on O_3 behavior in the BMR is examined by performing a sensitivity analysis of NO_x and VOC reductions in China's emissions, since China is a major contributor of pollutants in Asia. Four emission control strategies for China including 10 %, 20 %, and 40 % NO_x emission reductions, and 40 % NO_x emission reduction along with 40 % VOC emission reduction over China's region are examined for the sensitivity analysis (Table 2). The 10 % NO_x emission reduction is set as Strategy 1, regarding the national reduction target during China's 12th FYP for NO_x. The other two NO_x-only control strategies (20 % and 40 % NO_x emission reductions) are set as Strategy 2 and 3, respectively, to examine the responses of O_3 and its precursors in the BMR due to different China's NO_x emission reductions. The 40 % NO_x emission along with 40 % VOC emission reduction proposed by Wang and Hao (2012) is set as Strategy 4, in order to investigate implications for incorporating VOC emission reduction strategies in China.

2.4 Model evaluation protocol

Several discrete statistics, including the correlation coefficient (r), mean bias (MB), root mean square error (RMSE), and normalized mean bias (NMB) are used to evaluate the model baseline simulation for temperature (T), wind speed (WS), relative humidity (RH), pressure (P), and O_3 mixing ratio during daytime hours (10:00 to 17:00 local time [LT]). This time window was selected to avoid pollution accumulation by surface inversions (Pochanart et al., 2001; Uttamang et al., 2018). Hourly meteorology and daily maximum 8-hour-average O_3 mixing ratios (Max 8-h O_3) from 16 Pollution Control Department (PCD) Thailand monitoring stations located in and around the BMR region (Fig. 2) were compared with the simulated variables from the lowest model layer of d03. Details of the PCD monitoring stations equipment are provided in (Uttamang et al., 2018). A mean normalized bias error (MNBE) was applied instead of NMB for the O_3 mixing ratios evaluation, as the U.S. EPA suggests a MNBE criteria of ±10 to 15 % for regulatory modeling applications (Žabkar et al., 2013).

$$\text{MNBE} = \frac{1}{N}\sum\left(\frac{M_i - O_i}{O_i}\right) \times 100\ \%$$

Where M_i = modeled value i, O_i = observed value i, N = number of paired observed-modeled values.

The comparison between the simulations and the observations are provided using geo-reference information (latitude and longitude) of the monitoring stations.

196 **3. Results of model evaluation**

197 **3.1 Model evaluation during the 2010 dry season**

198 Table 3 summarizes the average January to March 2010 model evaluations of meteorology
199 and Max 8-h O_3 mixing ratios. The comparison between hourly simulated T, RH, P and WS in d03
200 with the observations from 16 monitoring stations show that the model accurately captures the
201 variations of T ($\bar{r}$ = ~0.8), RH ($\bar{r}$ = ~ 0.7) and P ($\bar{r}$ = ~ 0.8), but less accurately captures the
202 variations of WS ($\bar{r}$ = ~ 0.2). Overall, the model tends to underpredict T, RH, and P with negative
203 $\overline{MB}$ (T is ~ -2.8 °C, RH is -6.8 % and P is -1.5 hPa). For WS, overall, the model tends to overpredict
204 WS with $\overline{MB}$ is ~ 1.5 ms^{-1}.

205 The underpredicted T and RH and overpredicted WS in the WRF model has been reported
206 in other studies (Yerramilli et al., 2010). Yerramilli et al. (2010) also studied the effects of the
207 planetary boundary layer (PBL) and land surface model (LSM) physics in WRF-Chem simulations
208 of surface O_3 mixing ratios in the Central Gulf Coast region, southeast US. The results from their
209 study indicated that a similar combination of the YSU-PBL and Noah-LSM schemes (Table 1)
210 provided the best simulation of winds, temperature, humidity, mixed layer depth and O_3 mixing
211 ratios diurnal variations, but the model normally underpredicted O_3 mixing ratios and temperature
212 and overpredicted winds. WS are typically overpredicted in WRF due to unresolved topographical
213 features and an underestimated surface drag parameterization in the model at these scales
214 (Georgiou et al., 2018; Kumar et al., 2016; Yahya et al., 2014).

215 The evaluation of the daily Max 8-h O_3 mixing ratios show that across the different stations
216 in and around the BMR, the total averages of observed and simulated daily Max 8-h O_3 are 25.8 ±
217 9.8 ppb, and 20.8 ± 14.4 ppb, respectively. The *r* correlation ranges from -0.3 to 0.6, MB from -
218 24 to 15 ppb, RMSE from 12 to 57 ppb, and MNBE from -75 to 95 %. Large discrepancies and
219 poor correlations that affect the statistical ranges are strongly impacted by the sites in coastal areas
220 (at 19T, 26T, 27T and 34T monitoring station) and 60T monitoring station.Specifically for the
221 other monitoring stations (19T, 26T, 27T, 34T and 60T are excluded), the model underpredicts
222 daily Max 8-h O_3 with a $\overline{MB}$ of ~ -2 ppb a $\overline{RMSE}$ of ~ 17.6 ppb and $\overline{MNBE}$ of ~ -3.2%.

223 The baseline evaluation results show that the WRF-Chem model reasonably predicts the
224 meteorological variables, except for WS, and overpredicts WS for all monitoring stations. The
225 model performance for daily Max 8-hr O_3 predications near coastal areas are not good, but for
226 other monitoring stations, the model overall provides good performance (i.e., MNBE < ± 10%).

227 **3.2 Model evaluation during the O_3 event (5 to 6 March 2010) in the BMR**

228 On 5 to 6 March 2010, O_3 exceedances were observed at nine monitoring stations located
229 in the BMR (six monitoring stations are located in Bangkok (BKK) including 3T, 10T, 11T, 15T,
230 52T and 61T sites, and three monitoring stations are located in the outskirts of BKK including
231 14T, 22T and 27T site). The exceedances observed across the different monitoring sites ranged in
232 mixing ratio from 101 to 169 ppb. This period contained the highest hourly O_3 mixing ratios
233 observed (169 ppb) in 2010.

234 Figure 3 shows the comparison between the hourly observed and simulated O_3 mixing
235 ratios at the nine BMR monitoring stations before (1 to 4 March 2010) and during the O_3 event (5

to 6 March 2010). The model shows an ability to capture the O_3 event and reasonably reproduce the diurnal variations of O_3 at all the monitoring stations during the event. The hourly simulated O_3 is frequently underpredicted in the evening and the early morning (19:00 to 7:00 LT), but overpredicted during afternoon (13:00 to 18:00 LT). Across the sites the correlation coefficients range from 0.58 to 0.89 ($\bar{r}$ is ~ 0.8), MBs range from -24 to 10.2 ppb ($\overline{MB}$ is ~ -11.2 ppb), RMSEs range from 28.7 to 41.4 ppb ($\overline{RMSE}$ is ~ 35.5 ppb) and MNBEs range from -62.4 to -19.1 % ($\overline{MNBE}$ is ~ -44.2 %).

3.3 Spatial distribution of O_3 from baseline simulation

Figure 4 shows spatial distributions of simulated daytime O_3 in d01 ("regional" scale; top panels) and in d03 ("local" scale; bottom panels) from the baseline simulation. The monthly-average spatial distributions of O_3 over East Asia and Southeast Asia shows an increase of O_3 mixing ratios from January to March where the domain-wide monthly-average O_3 is 37.9 ± 12.1 ppb in January, 40.3 ± 12.7 ppb in February , 43.3 ± 12.9 ppb in March and the episodic-average is 43.6 ± 17.8 ppb (Fig. 4 (a)-(d)). Strong gradients of O_3 occurred from western China (the Tibetan Plateau) to eastern China. Ni et al. (2018) reported a similar pattern of O_3 over China during the spring 2008, in which the O_3 mixing ratios over the southern Tibetan Plateau ranged from 75 to 80 ppb and those over the North China Plain ranged from 25 to 40 ppb. Their study suggested that ~ 80 to 90% of O_3 mixing ratios over Tibet (low anthropogenic emissions) were contributed by biogenic O_3 precursors sources.

Our baseline simulation shows that local O_3 (d03) generally increases from January to March. The domain-wide monthly-average of O_3 are ~ 30 ppb in January, ~ 50 ppb in February, ~ 61 ppb in March and the episodic-average is ~ 67 ppb (Fig 4 (e)-(h)). Very high O_3 mixing ratios frequently occur over the Tenasserim range (the west of the domain) and hilly regions (the southeast of the domain).

3.4 Spatial distribution of O_3 precursors

Table S1.1 and S1.2 summarize the domain-wide monthly- and episodic-average mixing ratios of NO_x, CO, VOC, PAN, nitric acid (HNO_3), and total odd oxygen (where $O_x = O_3 + NO_2 + 2 \times$ nitrogen trioxide (NO_3) + HNO_3 + PAN) in the regional (d01), and local (d03) scales.

The regional (d01) spatial distributions of NO_x are similar to its emission sources (Fig. 5a)). High mixing ratios of NO_x are present over east China and the central region of Thailand (including the BMR), while very low mixing ratios are present over remote areas of the region. Spatial distributions of pollutants are effectively controlled by their lifetimes. Therefore, for a short lifetime species, for example, NO_x, high mixing ratios are normally confined near the emission sources (Amnuaylojaroen et al., 2014). The domain-wide monthly-average NO_x shows a decrease in NO_x from January to March, from ~52 ppb in January to ~25 ppb in March, but a higher value during the episodic-average of ~44 ppb. There are also high mixing ratios of CO near their source regions. CO has a longer lifetime (~1 month) than NO_x, however, and thus CO can be transported continentally and contribute to both regional and global burdens (NASA, 2014). CO decreases from January to March, from ~199 ppb in January to ~173 ppb in March, but also has a higher value for the episodic-average of ~200 ppb. High mixing ratios of VOC occur near source regions of both anthropogenic (i.e. east China, the central region of Thailand and eastern India [Fig 5b)])

and biogenic sources (i.e. Malaysia and Indonesia). where the total VOCs range from ~8 to ~9 ppb during January to March. PAN is a nitrogen reservoir species, which may be transported over distances and release NO_x away from its source (Jacob, 1999). The mixing ratios of PAN in a clean environment are ~2 to ~100 ppt and in polluted air are ~10 to ~20 ppb (Jacobson, 2012). In our study, high mixing ratios of PAN occur over Burma, Thailand, Malaysia and Indonesia, and can range on average from ~0.5 to ~0.7 ppb during January to March (Fig S1.2). HNO_3 is formed from the reaction of OH and NO_2 during daytime (Jiménez et al., 2012), and our model simulations suggest high mixing ratios of HNO_3 over east China and Thailand, ranging from ~3 to ~3.5 ppb during January to March.

On the local scale (d03), there are high mixing ratios of CO and NO_x around the BMR. The domain-wide monthly-average CO, NO_x and O_x mixing ratios decrease from January to March, and range from ~300 ppb for CO, ~121 ppb for NO_x and ~162 ppb for O_x in January, ~259 ppb for CO, ~93 ppb for NO_x and ~ 161 for O_x in February, ~224 ppb for CO, ~74 ppb for NO_x and ~151 for O_x during March and the episodic-average are ~242 ppb for CO and ~76 ppb for NO_x.

There are locally widespread high values of VOC and HNO_3 for all months, while the highest mixing ratios of PAN are over the Tenasserim range to the west, and over the mountainous areas on the east and southeast of the BMR. The domain-wide monthly-average VOC, PAN and HNO_3 mixing ratios increase from January to March, on average ranging from ~28 to ~31 ppb for VOC, ~0.4 to ~1.2 ppb for PAN and ~10.6 to ~15.3 ppb for HNO_3

Spatial distribution of domain-wide (d03) monthly-average delta NO_x, CO, VOC, PAN and HNO_3 are shown in supplement material (Fig. S1.1 to S1.4).

4. Results from sensitivity analysis

Figure 5 shows monthly-average NO_x and VOC emissions in January, February and March and the absolute differences (sensitivity – baseline) of the four NO_x and VOC emission reduction strategies (i.e 10 %, 20 %, and 40 % NO_x emission reductions, and 40 % NO_x emission reductions along with 40 % VOC emission reduction). Figure 6 shows monthly average wind fields in the outermost domain that are generated from the baseline simulation.

4.1 Effects on regional-scale O_3 precursors and O_3

The decreases in NO_x emissions over China (S1, S2, and S3) lead to NO_x mixing ratio reductions in eastern China during all the months, while there are some localized increases in NO_x levels over the central areas of Thailand in February and March. Table 4 summarizes delta (delta of species i, (X_i) = monthly-average $X_{i,reduction\_strategies}$ – monthly-average $X_{i,baseline}$) O_3 and its precursors, including NO_x, CO, VOC, PAN, HNO_3 and O_x in the regional scale (d01) due to China's emission reductions. There are widespread decreases in domain-wide monthly-average delta NO_x, on the order of about ~ 2.4 to 20.5 ppb (~ 10 to 40 %) compared with the baseline simulation . There are minor decreases in CO mixing ratios in eastern China, but slight increases in central Thailand . The domain-wide monthly-average delta CO are approximately ~ -0.5 to 0.03 ppb (~ -0.1 to 0 %). Moderate VOC reductions mostly occur in eastern China due to S4, which are approximately ~ 0.2 to ~ 1.0 ppb (~ 7 to 14 %) during January to March (Fig S3.3). There is a moderate increase in PAN due to decreased NO_x emissions, with increases approximately ~ 0.01

317 to 0.03 ppb (~ 1 to 7 %). PAN increases are mitigated, however when incorporating the 40 % VOC
318 emission reduction compared to the NO_x-only control strategies, with average changes of
319 approximately ~ 0.01 ppb (2 %) . HNO_3 mixing ratios are also reduced by ~ 0.1 to ~ 0.5 ppb (~
320 2% to 14 %) due to the NO_x emission reductions . O_x mixing ratios are also reduced by about ~
321 0.9 to 7.8 ppb (~ 1.5 to 11.5 %) due to the NO_x emission reductions; however, the O_x decreases (~
322 0.3 to 0.4 %) are significantly mitigated by including both 40 % NO_x and VOC emission reduction
323 compared to the NO_x-only strategy . Spatial distribution of domain-wide (d01) monthly-average
324 delta NO_x, CO, VOC, PAN and HNO_3 are shown in supplement material (Fig. S3.1 to S3.5).

325 The decreases in NO_x emissions over China (S1, S2, and S3) slightly increase the
326 monthly-average O_3 mixing ratios on the regional scale ~ 0.3 to 2 ppb (~1 % to ~5 %) from the
327 baseline simulation) perhaps owing to the region being VOC limited (Fig. 7). The spatial
328 distributions of monthly-average delta O_3 shows moderate increases in O_3 mixing ratios from
329 eastern China to southeast Asia in NE/SW directions. The domain-wide monthly-average delta
330 O_3 during January to March are ~ 0.3 to 0.4 ppb (0.7 to 0.9%) in S1, ~ 0.6 to 0.7 ppb (1.3 to 1.9
331 %) in S2,~ 1.2 to 1.5 ppb (2.7 to 4.1 %) in S3, and ~ 0.2 to 0.6 ppb (0.4 to 0.5 %) in S4. The
332 comparison between S3 and S4 shows that the combined 40 % NO_x and VOC emission reduction
333 acts to mitigate the O_3 increases compared with S3 (NO_x-only reductions), and further
334 demonstrates the implications for including VOC emission reduction strategies in China. The
335 changes of O_3 mixing ratio in the regional scale correlate with the changes of PAN mixing ratio
336 (increases in PAN increases in O_3).

337 The increase in the mixing ratios of O_3 and PAN (in a VOC-limited regime, a reduction
338 of NO_x lead to an increasing of PAN mixing ratios [Jiménez et al., 2012]) due to the 10 to 40 %
339 NO_x emission reduction strategies suggest that eastern China and northern Thailand are likely
340 VOC-limited during January to March, while some areas of central Thailand are VOC-limited
341 during January to February and become less VOC-limited in March. This is further supported by
342 the mitigation in O_3 increases when including both 40 % decreases in NO_x and VOC emissions
343 compared to the NO_x-only strategy. The results in this section also indicate the significance of
344 China's emission reductions on regional-scale pollution, as far as southern Thailand and the
345 BMR region.

346 **4.2 Effects on BMR O_3 pollution**

347 It was previously shown that emission reductions affect the regional-scale (d01) average
348 O_3 and its precursor mixing ratios. In this case, we analyze these effects on the local-scale (d03)
349 O_3 and precursor mixing ratios in the BMR.

350 Table 5 summarizes delta O_3 and its precursors in the local scale due to China's
351 emission reductions. The NO_x-only control strategies in China generally lead to decreases in
352 domain-wide monthly-average delta NO_x in January and February, on the order of ~ 3 to 19 ppb
353 (~ 1 to 9 %) from the baseline simulation, but moderate increases in the central regions of the
354 domain (including northwestern BMR) in March, on the order of ~ 22 to 28 ppb (~ 8 to 9 %) .
355 There are minor increases in CO (< 11 ppb) and VOC (< 1.4 ppb) mixing ratios in January and
356 February, on the order of < 1.5 %, and moderate increases in those species in the central regions
357 of the domain in March (~ 36 to 40 ppb [~ 6.0 to 6.5 %] for domain-wide monthly-average delta

CO and ~ 4 to 6 ppb [~ 4 to 5 %] for domain-wide monthly-average delta VOC). There are increases in PAN due to the NO_x-only control strategies, with increases ~ 0.01 to 0.12 ppb (~1 to 6 %). There are minor increases in domain-wide monthly-average delta HNO_3 in January, on the order of ~ 0.03 to 0.14 ppb (~ 0.6 to 3 %), but widespread decreases (~ 0.2 to 0.5 ppb [< 4 %]) in this species in February. In March, the reduction of HNO_3 mostly occurs in central domain (~ 0.4 to 0.5 ppb [~ 3 to 4 %] for domain-wide monthly-average delta HNO_3). Widespread increase in O_x occur for all the months, on the order of ~ 1.1 to 6.1 ppb (~ 0.5 to 2 %). The modeling difference between S3 (40% China's emission reduction) and S4 (NO_x and VOC reduction each by 40%) shows that O_3 precursors (i.e. CO, HNO_3, PAN and O_x) mixing ratios are mitigated during January and February; while in March, the incorporating of VOC reduction (S4) does not reduce the mixing ratio of the O_3 precursors. Spatial distribution of domain-wide (d03) monthly-average delta NO_x, CO, VOC, PAN and HNO_3 are shown in supplement material (Fig. S3.7 to S3.12).

The NO_x-only control strategies in China mostly increase the monthly-average O_3 mixing ratios on the local scale (d03), on the order of 0.1 to 3 ppb (~ 1 to 6 %) from the baseline simulation (Fig. 8). The distributions of monthly-average delta O_3 shows widespread increase in O_3 mixing ratios in January and February, but some O_3 reductions occur in the central areas of the domain (including northern BMR). The domain-wide monthly-average delta O_3 during January to March are ~ -0.34 to 3.0 ppb (-0.4 to ~ 2 %) in S1, ~ 0.2 to 2.0 ppb (~ 0.2 to 3.5 %) in S2, ~ 1.0 to 3.0 ppb (~ 1 to 6 %) in S3, and ~1.0 to 3.0 ppb (~ 1 to 7 %) in S4. The comparison between S3 and S4 shows that the combined 40 % NO_x and VOC emission reduction acts to slightly mitigate the O_3 increases compared with S3 in January and February, but the VOC emission reduction does not improve the O_3 levels in March. The increases in the mixing ratios of O_3 and PAN due to the NO_x-only control strategies suggest that the central, western and eastern regions of Thailand are likely VOC-limited during January to February. However, in March, the increases in O_3 are not mitigated by the reductions of VOC suggesting that these areas become less VOC-limited in this month.

Figure 9 illustrates the changes of delta O_3 due to the China's emission control strategies at 10 monitoring stations located in the BMR (3T, 10T, 11T, 14T, 15T, 19T, 22T, 27T, 52T and 61T sites). In January and February (Fig. 9a) to 9b)), NO_x emission reduction mostly increases the monthly-average mixing ratio of O_3. However, incorporating 40 % VOC emission reduction in China decreases O_3 at most monitoring stations. During March (Fig. 9c)), NO_x emission reduction in China enhance the mixing ratio of O_3 at 14T, 19T, 22T, and 27T monitoring stations. However, the increases in O_3 are mitigated by 40% VOC emission reduction in China. On the other hand, the NO_x-only control strategies reduce the mixing ratios of O_3 at 3T, 10T, 11T, 52T and 61T monitoring stations, while incorporating 40 % VOC reduction increases O_3 levels at most sites (Fig. 9c)). The results in this section further support that the BMR is VOC-limited in January and February, on the other hand, this area becomes less VOC-limited or even NO_x-limited in March in some parts of the BMR (NRC, 1991).

5. Analysis of NO_x-VOC indicators of O_3 formation

There are several photochemical indicators used to predict NO_x- and VOC-limited O_3 formation regimes including H_2O_2/HNO_3, O_3/NO_x, O_3/NO_y (where $NOy = NO_x + HNO_3 + N_2O_5 + NO_3 + PAN + HONO + HNO_4$), O_3/NO_z (where $NO_z = HNO_3 + N_2O_5 + NO_3 + PAN + HONO +$

399 HNO_4), HCHO/NO_2 and HCHO/NO_y (Sillman, 1995; Hammer et al., 2002; Lam et al., 2005;
400 Zhang et al., 2009; Campbell et al., 2015). The ratio of H_2O_2/HNO_3 is an important indicator of
401 NO_x- and VOC-limited regimes of O_3 formation (Lam et al., 2005 and Hammer et al., 2002). Under
402 low NO_x mixing ratios, H_2O_2 is the major radical sink, while HNO_3 is the major radical sink under
403 high NO_x mixing ratios. Therefore, a high and low ratio of H_2O_2/HNO_3 indicate a NO_x-limited
404 regime and a VOC-limited regime, respectively (Lam et al., 2005 and Jacob, 1999). The transition
405 value of H_2O_2/HNO_3 is 0.2 (Hammer et al., 2002; Lam et al., 2005; Liu et al., 2010; Sillman, 1995;
406 Zhang et al., 2009). When a value is lower than the transition value, a VOC-limited regime is more
407 indicated; otherwise, NO_x-limited regime is may be favored (Lam et al., 2005).

408 Figure 10a) to 10d) illustrate the spatial distributions of monthly-average H_2O_2/HNO_3 in
409 the regional scale during daytime (10:00 to 17:00 LT) with the transition value of 0.2. The spatial
410 distributions indicate that, in January, the majority of this region is NO_x-limited, except for
411 southern China, northwestern China, eastern India and some regions of Thailand (central and
412 northern Thailand), where those areas are VOC-limited. During February to March, most of
413 eastern China tends to become more VOC-limited; however, big cities (i.e. Beijing and Shanghai)
414 continue to remain NO_x-limited.

415 Figure 10e) to 10h) show the spatial distributions of monthly-average and O_3-event-period-
416 average H_2O_2/HNO_3 on the local-scale (d03) during daytime with the transitional value of 0.2. The
417 spatial distributions of the indicator suggest that during January to February, nearly the entire
418 domain, including the BMR, are VOC-limited. During March, the central regions of the domain
419 becomes NO_x-limited.

420 The VOC-NO_x indicator for the formation of ozone support the results in section 5 (the
421 change of O_3 mixing ratios due to China's NO_x and VOC emission reductions); which, in general,
422 cover eastern China and northern to central Thailand including the BMR, are likely VOC-limited.
423 However, in March, reversals from VOC-limited to NO_x-limited may be found in some parts of
424 the BMR.

425 **6. Effects of local flows and topography on O_3 levels in the BMR.**

426 China's emission control strategies affect regional and local chemical species, including
427 O_3 and its precursors. These effects are more obvious in March than in the other months. The
428 indicator analysis suggested that in the northeastern and eastern regions of China, and the central
429 areas of Thailand and the BMR, are normally in VOC-limited which a decrease in NO_x emissions
430 lead to an increase in O_3. In this section, we examine possible processes affecting O_3 formation,
431 accumulation and transport in this area, especially local flows and topography in the innermost
432 domain, since this domain has a very complex topography (flat terrain in the center, the Tenasserim
433 range on the west, mountainous areas on the east and southeast, and coastal areas and sea over the
434 south). The complex topography of the innermost domain produces a flow channeling in valleys
435 and very complicated flow structures due to the superposition of the different scale of flows (i.e.
436 mountain winds, breezes and flows from nonuniform land use) that influence mixing ratios, and
437 model simulation accuracy (Gustin et al., 2015; Jiménez et al., 2012).

438 We investigate the diurnal cycle of O_3 against wind vector in the lowest model layer during
439 the O_3 event (5 to 6 March 2010) to describe the pollution dynamics and examine the effects of

local flows on pollutants mixing ratios in d03. Figure 11 illustrates the dynamics of the daily cycle of O_3 in d03. In the early morning (5:00 LT), mountain winds from the Tenasserim range and the mountainous areas, and land- and sea-breeze circulations around the coastal areas help establishing south-north flows over the flat plain. At this time, there are widespread low O_3 mixing ratios, while higher O_3 mixing ratios are found around the mountainous areas, and around the coastal areas on the south. Since there is no new O_3 is formed during this time, the spatial distribution of O_3 shows the effect of topography (i.e. mountainous areas) on O_3 accumulation, and the effect of local flows (i.e. land- and sea-breeze circulations) on O_3 transport, which the circulation recirculates O_3 to inland. During 10:00 to 14:00 LT, the transition between sea- and land-breeze occurs over the gulf of Thailand. Strong sea-breezes are the dominant flow over the coastal areas and penetrate the inland. During this time, there are widespread increases in O_3 with high O_3 mixing ratios, which are mostly found over the Tenasserim range and the mountainous areas, where biogenic VOC (BVOC) emissions are high. The presence of BVOC emissions favor the formation of O_3 (Chatani et al., 2015; Sillman, 1999) in this area, since the indicators analysis show that this area is VOC-limited. O_3 and BVOC from the Tenasserim range are transported to the flat terrain by mountain winds, which later converge with the sea-breezes and bring the pollutants to the northern regions of the domain. In the late afternoon to the evening (18:00 to 23:00 LT), the mixing ratios of O_3 start decreasing due to a lack of sunlight to promote photochemical reactions, the titration of O_3 by NO at night (Jiménez et al., 2012; Tokarek et al., 2017) and the reaction of O_3 with unsaturated biogenic hydrocarbons (Tokarek et al., 2017). These O_3 depletion mechanisms are further supported by the diurnal cycles of VOC, NO and NO_2. At night, the increases in NO_2 are mostly found over the central areas of the domain, while the mixing ratios of NO is near zero. A combination of the presence of high VOC, especially over the flat terrain and strong sea-breezes during nighttime, may be a cause of underpredicted O_3 at night over this area (d03), especially at coastal monitoring stations (i.e. 19T and 27T station). Spatial distribution of O_3, BVOC, NO and NO_2 during the O_3 event are shown in the supplement material (Fig. S4.1 to S4.4).

7. Summary and discussion

We examine O_3 behavior and the influence of China's NO_x and VOC emissions and the subsequent transport of O_3 and O_3 precursors on O_3 levels in the BMR by the WRF-Chem model, since elevated O_3 in the BMR was affected by both local and regional contribution of precursor pollutants. Generally, the model reasonably predicts O_3 mixing ratios and performs well in capturing the O_3 event. During the O_3 season, the decreases in China's NO_x emissions (10 %, 20 %, and 40 % NO_x emission reductions) lead to decreases in the regional O_3 precursors (i.e. NO_x, CO, VOC, HNO_3 and O_x), but increases in the regional PAN and O_3. The increases in PAN and O_3 are mitigated by incorporating 40 % China's VOC emission reduction.

The NO_x-only emission reductions in China mostly lead to widespread increases in local scale (d03) O_3 and O_3 precursors (except NO_x that the minor decreases are found in January and February), while incorporating 40 % China's VOC emission reduction mostly decrease O_3 mixing ratios in this area. The increase in the mixing ratios of O_3 and PAN in the regional- and local-scale, including the BMR, due to the NO_x-only emission reductions in China suggest that eastern China and northern to central Thailand are likely VOC-limited; however, in March, these regions become less VOC-limited. This is further supported by the mitigation in O_3 increases when including 40

% VOC emissions reduction and by the results from the indicator analysis. The discrepancy between O_3/NO_z and the other indicator may come from very low simulated mixing ratios of NO_z (approximately on the order of 10^{-2} to 10^{-3} ppb), although we do not have an observation to compare with the simulation for this species.

A change of VOC- and NO_x-limited regime may occur due to i) Emissions intensity, ii) Cumulative solar radiation, iii) Intensity of solar radiation, and iv) VOC reactivity (Kannari and Ohara, 2010). However, the use of modeled O_3 photochemical indicators averaged over regional and monthly-to-seasonal time scales has been shown to be a well-established method used to differentiate between NO_x- and VOC-limited O_3 chemical regimes, which are based on transition values in North America (Zhang et al., 2009, Campbell et al., 2015), Europe (Walaszek et al., 2017), and Asia (Liu et al., 2010). While the split between NO_x- and VOC-limited conditions may indeed shift in space and time (as explained above) the use of particular O_3 indicator ratios are valid tools for diagnosing if NO_x or VOC emission controls are beneficial or detrimental (Liang et al., 2006; Jin et al., 2017; Walaszek et al., 2017). It is noteworthy that ambient O_3 mixing ratios have a complex nonlinear relationship with VOC and NO_x mixtures; therefore, it is important that the emission inventories be accurate (Fujita et al., 2013).

Our study depicts that China's emissions play an important role in controlling the pollutant levels in this region. The changes in regional NO_x mixing ratios correspond directly to the changes of China's NO_x emissions; however, controlling only NO_x emissions is not an effective strategy to reduce O_3 mixing ratios in this region. The change in regional VOC mixing ratios varied from the changes in China's VOC emission reduction. Therefore, the regional VOC mixing ratios is perhaps influenced by other VOC emission sources (i.e. biogenic VOC emission sources) where the decreases in VOC emissions provide additional benefits for controlling O_3 mixing ratios.

In the BMR, our analysis suggests that not only local anthropogenic emissions, but also long-range transport of pollutants, as far as originating from China, influence O_3 formation in the BMR. Results from this study with different scenarios show that the WRF-Chem model could be a useful tool to evaluate O_3 formation and the relationship between O_3-NO_x-VOCs and O_3 formation in the BMR; however, the practical implementation or control strategies based on this study are complicated. It is difficult to quantify the proportion of pollutants contributing to local emissions and from those associated with long-range transport due to the lack of emission data in the BMR. BVOC transported from the Tenasserim range by mountain winds also favor the O_3 formation in this area; since this area is indicated as a VOC-limited regime, the increases in VOC lead to the increases in O_3 levels. Another factor influences O_3 and its precursors levels is land and sea-breeze circulations over the Gulf of Thailand, which the circulations do not only dilute the mixing ratios over the east side of coastal areas, but may also recirculate pollutants to inland, resulting in the increases in pollutants level. Thus, issues associated with the complex terrain and coastal vicinity of some of the sites may prevent the model from having accurate predictions.

It must be emphasized that uncertainties in this study may be from uncertainties in biogenic and anthropogenic emissions. In general, uncertainties in spatial input (i.e. land use, plant functional type and leaf area index) contribute to the accuracy of biogenic emission estimation, tropospheric O_3 and its precursors variation (Porter and Heald, 2019). For

anthropogenic emission inventories, uncertainties in regional emissions may be expected as large as a factor of 2 or even larger (Bond et al. (2004, 2007); Smith et al. (2010)). Uncertainties may come from meteorological simulation and chemistry from the WRF-Chem model. In general, windspeed is more likely to be the largest source of uncertainty; however, chemical reaction rates and stoichiometry may also be a major cause of simulated O_3 uncertainty (~20%) (Sillman, 1999). In our study, the finest horizontal resolution is 4 km which may be too coarse to deal with very complicated flow structures. Jiménez et al. (2012) suggested that a high-resolution model (resolution of $\leq$ 1 km) was required in order to study air pollution in a very complex topography. However, the high-resolution model had to be nested in a larger model domain in order to investigate the effects of larger-scale transport.

Simulated NO_x and VOCs analysis offers important information to distinguish the ozone—precursor relationship in terms of a split between a NO_x-limited and VOCs-limited regimes (or NO_x -saturated). However, the simulations of these species are also subject to large uncertainties. Sillman (1999) reported five factors that influenced estimated NO_x- and VOCs-limited regimes were i) VOC/NO_x ratios, ii) VOC reactivity, iii) biogenic hydrocarbons, iv) photochemical aging of the air mass, and v) rates of meteorological dispersion. Furthermore, this study examines the formation of O_3 in the BMR primarily during January to March (dry season), and the model evaluations are also done during the same study period. However, the study on O_3 formation and model evaluation need to be extended for at least a complete one-year study.

This article presents insights derived from WRF-Chem model and field measurements in BMR; and seeks to demonstrate the relationships between ozone—NO_x —VOC chemistry and transport. This analysis of ozone—NO_x —VOC sensitivity has close connection to air quality management and regulatory policy for BMR.

Acknowledgments

We thank the Royal Thai Government for providing a fellowship to Pornpan Uttamang (ref. no.1018.2/4440). We thank the Air Quality and Noise Management Bureau, Pollution Control Department, Ministry of Natural Resources and Environment, Bangkok, Thailand, for use of providing QA/QC air pollution and meteorology data. We thank NCAR-UCAR CISL for Cheyenne, the high-performance computer. We also thank Dr. Gary Lackmann, the department of Marine Earth and Atmospheric Sciences, North Carolina State University and Dr. Chinmay Kumar Jena, Indian Institute of Tropical Meteorology for the model assistances. Finally, we thank Shannon Madden in the Graduate School at North Carolina State University for her assistance in manuscript preparation.

Disclaimer

The scientific results and conclusions, as well as any views or opinions expressed herein, are those of the author(s) and do not necessarily reflect the views of NOAA or the Department of Commerce.

Code and Data availability

The WRF-Chem model (all version) is available at WRF Users page (http://www2.mmm.ucar.edu/wrf/users/download/get_sources.html#WRF-Chem).

Meteorology data is available at NCAR UCAR Research Data Archive computational & Information System Lab website (https://rda.ucar.edu/).

Data to prepare initial and boundary conditions is available at NCAR UCAR Atmospheric Chemistry Observations & Modeling website (https://www.acom.ucar.edu/wrf-chem/mozart.shtml).

EDGAR-HTAP data is available at European Commission, joint Research Center, EDGAR-Emissions Database for Global Atmospheric Research (https://edgar.jrc.ec.europa.eu/).

Scripts in this study are written in the NCAR Command Language (NCL). The program is available at GitHub NCAR/ncl (https://github.com/NCAR/ncl). More information about NCL can be found at http://www.ncl.ucar.edu/.

Data is available with the primary author.

References

Amnuaylojaroen, T., Barth, M.C., Emmons, L.K., Carmichael, G.R., Kreasuwun, J., Prasitwattanaseree, S., 2014. Effect of different emission inventories on modeled ozone and carbon monoxide in Southeast Asia 12983–13012. https://doi.org/10.5194/acp-14-12983-2014

Bond, T. C., Streets, D. G., Yarber, K. F., Nelson, S. M., Woo, J.-H., Klimont, Z., 2004. A Technology-Based Global Inventory of Black and Organic Carbon Emissions from

595 Combustion, J Geophys. Res., 109, D14203, doi:10.1029/2003JD003697

596 Bond, T. C., Bhardwaj, E., Dong, R., Jogani, R., Jung, S., Roden, C., Streets, D. G., and
597 Trautmann, N. M., 2007. Historical emissions of black and organic carbon aerosol from
598 energy-related combustion, 1850–2000, Global Biogeochem. Cy., 21, GB2018,
599 doi:10.1029/2006GB002840

600 Bucher, J.R., Thayer, K., Birnbaum, L.S., 2011. The office of health assessment and translation:
601 A problem-solving resource for the national toxicology program. Environ. Health Perspect.
602 119, 196–198. https://doi.org/10.1289/ehp.1103645

603 Campbell, P., Zhang, Y., Yahya, K., Wang, K., Hogrefe, C., Pouliot, G., Knote, C., Hodzic, A.,
604 San Jose, R., Perez, J.L., Jimenez Guerrero, P., Baro, R., Makar, P., 2015. A multi-model
605 assessment for the 2006 and 2010 simulations under the Air Quality Model Evaluation
606 International Initiative (AQMEII) phase 2 over North America: Part I. Indicators of the
607 sensitivity of O3 and PM2.5 formation regimes. Atmos. Environ. 115, 569–586

608 Chatani, S., Matsunaga, S.N., Nakatsuka, S., 2015. Estimate of biogenic VOC emissions in Japan
609 and their effects on photochemical formation of ambient ozone and secondary organic
610 aerosol. Atmos. Environ. 120, 38–50. https://doi.org/10.1016/j.atmosenv.2015.08.086

611 Chen, F., Dudhia, J., 2001. Coupling an Advance Land Surface-Hydrology Model with the Penn
612 State-NCAR MM5 Modeling System. Part I: Model Implement and Sensitivity. Mon.
613 Weather Rev. 129, 569–585.

614 Chueinta, W., Hopke, P.K., Paatero, P., 2000. Investigation of sources of atmospheric aerosol at
615 urban and suburban residential areas in Thailand by positive matrix factorization. Atmos.
616 Environ. 34, 3319–3329. https://doi.org/10.1016/S1352-2310(99)00433-1

617 Coates, J., Mar, K.A., Ojha, N., Butler, T.M., 2016. The influence of temperature on ozone
618 production under varying NO_x conditions - A modelling study. Atmos. Chem. Phys. 16,
619 11601–11615. https://doi.org/10.5194/acp-16-11601-2016

620 Cuesta, J., Kanaya, Y., Takigawa, M., Dufour, G., Eremenko, M., Foret, G., Systèmes, I., Lisa,
621 A., Créteil, U.P., 2018. Transboundary ozone pollution across East Asia: daily evolution
622 and photochemical production analysed by IASI + GOME2 multispectral satellite
623 observations and models 9499–9525.

624 Emmons, L.K., Walters, S., Hess, P.G., Lamarque, J.F., Pfister, G.G., Fillmore, D., Granier, C.,
625 Guenther, A., Kinnison, D., Laepple, T., Orlando, J., Tie, X., Tyndall, G., Wiedinmyer, C.,
626 Baughcum, S.L., Kloster, S., 2010. Description and evaluation of the Model for Ozone and
627 Related chemical Tracers, version 4 (MOZART-4). Geosci. Model Dev. 3, 43–67.
628 https://doi.org/10.5194/gmd-3-43-2010

629 Fairall, C.W., Bradley, E.F., Hare, J.E., Grachev, A.A., Edson, J.B., 2003. Bulk parameterization
630 of air-sea fluxes: Updates and verification for the COARE algorithm. J. Clim. 16, 571–591.
631 https://doi.org/10.1175/1520-0442(2003)016<0571:BPOASF>2.0.CO;2

632 Forkel, R., Werhahn, J., Buus, A., Mckeen, S., Peckham, S., Grell, G., Suppan, P., 2012. Effect
633 of aerosol-radiation feedback on regional air quality e A case study with WRF / Chem.

634 Atmos. Environ. 53, 202–211. https://doi.org/10.1016/j.atmosenv.2011.10.009

635 Fujita, E.M., Campbell, D.E., Stockwell, W.R., Lawson, D.R., 2013. Past and future ozone
636 trends in California's South Coast Air Basin: Reconciliation of ambient measurements with
637 past and projected emission inventories. J. Air Waste Manag. Assoc. 63, 54–69.
638 https://doi.org/10.1080/10962247.2012.735211

639 Georgiou, G.K., Christoudias, T., Proestos, Y., Kushta, J., Hadjinicolaou, P., Lelieveld, J., 2018.
640 Air quality modelling in the summer over the eastern Mediterranean using WRF-Chem:
641 Chemistry and aerosol mechanism intercomparison. Atmos. Chem. Phys. 18, 1555–1571.
642 https://doi.org/10.5194/acp-18-1555-2018

643 Grell, G.A., Freitas, S.R., 2014. A scale and aerosol aware stochastic convective
644 parameterization for weather and air quality modeling. Atmos. Chem. Phys. 14, 5233–5250.
645 https://doi.org/10.5194/acp-14-5233-2014

646 Grell, G.A., Peckham, S.E., Schmitz, R., McKeen, S.A., Frost, G., Skamarock, W.C., Eder, B.,
647 2005. Fully coupled "online" chemistry within the WRF model. Atmos. Environ. 39, 6957–
648 6975. https://doi.org/10.1016/j.atmosenv.2005.04.027

649 Guenther, A., Karl, T., Harley, P., Wiedinmyer, C., Palmer, P.I., Geron, C., 2006. and Physics
650 Estimates of global terrestrial isoprene emissions using MEGAN (Model of Emissions of
651 Gases and Aerosols from Nature). Atmos. Chem. Phys. 6, 3181–3210.

652 Guo, J., He, J., Liu, H., Miao, Y., Liu, H., Zhai, P., 2016. Impact of various emission control
653 schemes on air quality using WRF-Chem during APEC China 2014. Atmos. Environ. 140,
654 311–319. https://doi.org/10.1016/j.atmosenv.2016.05.046

655 Guo, S., Hu, M., Zamora, M.L., Peng, J., Shang, D., Zheng, J., Du, Z., Wu, Z., Shao, M., Zeng,
656 L., Molina, M.J., Zhang, R., 2014. Elucidating severe urban haze formation in China. Proc.
657 Natl. Acad. Sci. 111, 17373–17378. https://doi.org/10.1073/pnas.1419604111

658 Gustin, M.S., Fine, R., Miller, M., Jaffe, D., Burley, J., 2015. The Nevada Rural Ozone Initiative
659 (NVROI): Insights to understanding air pollution in complex terrain. Sci. Total Environ.
660 530–531, 455–470. https://doi.org/10.1016/j.scitotenv.2015.03.046

661 Hammer, M.U., Vogel, B., Vogel, H., 2002. Findings on H_2O_2/HNO_3 as an indicator of ozone
662 sensitivity in Baden-Württemberg, Berlin-Brandenburg, and the Po valley based on
663 numerical simulations. J. Geophys. Res. Atmos. 107, 1–18.
664 https://doi.org/10.1029/2000JD000211

665 Hong, S.-Y., Noh, Y., Dudhia, J., 2006. A New Vertical Diffusion Package with an Explicit
666 Treatment of Entrainment Processes. Mon. Weather Rev. 134, 2318–2341.
667 https://doi.org/10.1175/MWR3199.1

668 Iacono, M.J., Delamere, J.S., Mlawer, E.J., Shephard, M.W., Clough, S.A., Collins, W.D., 2008.
669 Radiative forcing by long-lived greenhouse gases: Calculations with the AER radiative
670 transfer models. J. Geophys. Res. Atmos. 113, 2–9. https://doi.org/10.1029/2008JD009944

671 Jacob, D.J., 1999. Introduction to atmopsheric chemistry. Princeton University Press, New

672 Jersey.

673 Jacobson, M.Z., 2012. Air pollution and global warming: history, science, and solutions, 2nd ed.
674 Cambridge University Press, New York.

675 Janssens-Maenhout, G., Dentener, F.J., Aardenne, J. Van, Monni, S., Pagliari, V., Orlandini, L.,
676 Klimont, Z., Kurokawa, J., Akimoto, H., Ohara, T., Wankmüller, R., Battye, B., Grano, D.,
677 Zuber, A., Keating, T., 2012. EDGAR-HTAP: a harmonized gridded air pollution emission
678 dataset based on national inventories, JRC Scientific and Technical Reports.
679 https://doi.org/10.2788/14102

680 Jiménez, P., Parra, R., Baldasano, J.M., 2012. Control of Ozone Precursors in a Complex
681 Industrial Terrain by Using Multiscale-Nested Air Quality Models with Fine Spatial
682 Resolution (1 km) Control of Ozone Precursors in a Complex Industrial Terrain by Using
683 Multiscale-Nested Air Quality Models with Fine Spatial Resolution (1 km^2) 2247.
684 https://doi.org/10.1080/10473289.2005.10464709

685 Jin, X., Fiore, A.M., Murray, L.T., Lukas, C.V., Lok, N.L., Bryan, D., Folkert, B., Isabelle, D.S.,
686 Gonzalo, G.A., Kelly, C., Gail S.T., 2017. Evaluating a Space-Based Indicator of Surface
687 Ozone-NOx -VOC Sensitivity Over Midlatitude Source Regions and Application to
688 Decadal Trends. J Geophys Res Atmos. 122(19), 10–461. doi:10.1002/2017JD02672.

689 Jose, R.S., Péreza, J.L., Gonzálezb, R.M., Peccic, J., Palacio, M., 2017. Improving air quality
690 modelling systems by usingon-line wild landfire forecasting tools coupledinto WRF/Chem
691 simulations over Europe. Urban Clim. 22, 2–18. https://doi.org/R.S. Jose)
692 http://dx.doi.org/10.1016/j.uclim.2016.09.001

693 Karagulian, F., Temimi, M., Ghebreyesus, D., Weston, M., Kondapalli, N.K., Valappil, V.K.,
694 Aldababesh, A., Lyapustin, A., Chaouch, N., Hammadi, F. Al, 2019. Analysis of a severe
695 dust storm and its impact on air quality conditions using WRF-Chem modeling, satellite
696 imagery, and ground observations. Air Qual. Atmos. Heal. 12, 453–470.

697 Kannari, A., Ohara, T., 2010. Theoretical implication of reversals of the ozone weekend effect
698 systematically observed in Japan. Atmos. Chem. Phys. 10, 6765–6776.
699 https://doi.org/10.5194/acp-10-6765-2010

700 Kim, Y.-J., Woo, J., Ma, Y., Kim, S., Sik, J., Sung, H., Choi, K., Seo, J., Su, J., Kang, C., Lee,
701 G., Ro, C., Chang, D., Sunwoo, Y., 2009. Chemical characteristics of long-range transport
702 aerosol at background sites in Korea. Atmos. Environ. 43, 5556–5566.
703 https://doi.org/10.1016/j.atmosenv.2009.03.062

704 Kumar, A., Jiménez, R., Belalcázar, L.C., Rojas, N.Y., 2016. Application of WRF-Chem model
705 to simulate PM10mixing ratio over Bogota. Aerosol Air Qual. Res. 16, 1206–1221.
706 https://doi.org/10.4209/aaqr.2015.05.0318

707 Lam, K.S., Wang, T.J., Wu, C.L., Li, Y.S., 2005. Study on an ozone episode in hot season in
708 Hong Kong and transboundary air pollution over Pearl River Delta region of China. Atmos.
709 Environ. 39, 1967–1977. https://doi.org/10.1016/j.atmosenv.2004.11.023

710 Lee, S., Ho, C., Gon, Y., Choi, H., Song, C., 2013. In fluence of transboundary air pollutants

711 from China on the high- PM 10 episode in Seoul, Korea for the period October 16 L 20,
712 2008. Atmos. Environ. 77, 430–439. https://doi.org/10.1016/j.atmosenv.2013.05.006

713 Lee, Y.C., Shindell, D.T., Faluvegi, G., Wenig, M., Lam, Y.F., Ning, Z., Hao, S., Lai, C.S.,
714 2014. Increase of ozone mixing ratios, its temperature sensitivity and the precursor factor in
715 South China. Tellus, Ser. B Chem. Phys. Meteorol. 66, 1–16.
716 https://doi.org/10.3402/tellusb.v66.23455

717 Liang, J., Bruce, J., Ajith, K., 2006. Evaluation of the ability of indicator species ratios to
718 determine the sensitivity of ozone to reductions in emissions of volatile organic compounds
719 and oxides of nitrogen in northern California, Atmospheric Environment. 40(27), 5156-
720 5166. https://doi.org/10.1016/j.atmosenv.2014.04.030.

721 Liang, X., Chen, X., Zhang, J., Shi, T., Sun, X., Fan, L., Wang, L., Ye, D., 2017. Reactivity-
722 based industrial volatile organic compounds emission inventory and its implications for
723 ozone control strategies in China. Atmos. Environ. 162, 115–126.
724 https://doi.org/10.1016/j.atmosenv.2017.04.036

725 Liu, X., Zhang, Y., Xing, J., Zhang, Q., Wang, K., Streets, D.G., Jang, C., Wang, W., Hao, J.,
726 2010. Understanding of regional air pollution over China using CMAQ, part II. Process
727 analysis and sensitivity of ozone and particulate matter to precursor emissions. Atmos.
728 Environ. 44, 3719–3727. https://doi.org/10.1016/j.atmosenv.2010.03.036

729 Liua, L., Huanga, X., Dinga, A., Fu, C., 2016. Dust-induced radiative feedbacks in north China:
730 A dust stormepisode modeling study using WRF-Chem. Atmos. Environ. 129, 43–54.
731 https://doi.org/http://dx.doi.org/10.106/j.atmosenv.2016.01.019

732 Millard, F., Toupance, G., 2002. Indicators concept applied to European city: the Ile de France
733 area during ESQUIF campaign, Air Pollution Modelling and Simulation. Springer, Berlin,
734 Heidelberg. https://doi.org/https://doi.org/10.1007/978-3-662-04956-3_7

735 NASA, 2014. Simulated Surface Carbon Monoxide [WWW Document]. URL
736 https://svs.gsfc.nasa.gov/30640

737 National Research Council (NRC), 1991. Rethinking the ozone problem in urban and regional air
738 pollution. National Academy Press, Washington, D.C.

739 Ni, R., Lin, J., Yan, Y., Lin, W., 2018. Foreign and domestic contributions to springtime ozone
740 over China 11447–11469.

741 Oanh, N.T. K, Upadhyay, N., Zhuang, Y.H., Hao, Z.P., Murthy, D.V.S., Lestari, P., Villarin,
742 J.T., Chengchua, K., Co, H.X., Dung, N.T., Lindgren, E.S., 2006. Particulate air pollution in
743 six Asian cities: Spatial and temporal distributions, and associated sources. Atmos. Environ.
744 40, 3367–3380. https://doi.org/10.1016/j.atmosenv.2006.01.050

745 Oanh, N.T.K., Zhang, B., 2004. Photochemical Smog Modeling for Assessment of Potential
746 Impacts of Different Management Strategies on Air Quality of the Bangkok Metropolitan
747 Region, Thailand. J. Air Waste Manag. Assoc. 54, 1321–1338.
748 https://doi.org/10.1016/j.apm.2017.04.042

749 Oh, H., Ho, C., Kim, J., Chen, D., Lee, S., Choi, Y., Chang, L., Song, C., 2015. Long-range

transport of air pollutants originating in China: A possible major cause of multi-day high-PM 10 episodes during cold season in Seoul, Korea. Atmos. Environ. 109, 23–30. https://doi.org/10.1016/j.atmosenv.2015.03.005

Oliveira, V., Freitas, S.R., Lima, R.S.S., Alonso, M.F., Bela, M.M., Fonseca, R., Gácita, M.S., Longo, K.M., Eiras, D., 2016. A preprocessor of trace gas and aerosol emission fields for regional and global atmospheric chemistry models.

PCD, 2018. National ambient air quality and Noise standards of Thailand [WWW Document]. URL http://www.pcd.go.th/info_serv/reg_std_airsnd01.html (accessed 1.13.19).

PCD, 2012. Thailand state of pollution 2012 [WWW Document], 2012. URL http://infofile.pcd.go.th/mgt/Report_Thai2555.pdf?CFID=208567&CFTOKEN=61191751 (accessed 1.31.20).

Pochanart, P., Kreasuwun, J., Sukasem, P., Geeratithadaniyom, W., Tabucanon, M.S., Hirokawa, J., Kajii, Y., Akimoto, H., 2001. Tropical tropospheric ozone observed in Thailand. Atmos. Environ. 35, 2657–2668. https://doi.org/10.1016/S1352-2310(00)00441-6

Podrascanin, Z., 2019. Setting-up a Real-Time Air Quality Forecasting system for Serbia: a WRF-Chem feasibility study with different horizontal resolutions and emission inventories. Environ. Sci. Pollut. Res.

Porter, W.C., Heald, C.L., 2019. The mechanisms and meteorological drivers of the summertime ozone–temperature relationship. Atmos. Chem. Phys., 19, 13367–13381. https://doi.org/10.5194/acp-19-13367-2019

Ruchirawat, M., Mahidol, C., Tangjarukij, C., Pui-ock, S., Jensen, O., Kampeerawipakorn, O., Tuntaviroon, J., Aramphongphan, A., Autrup, H., 2002. Exposure to genotoxins present in ambient air in Bangkok, Thailand - Particle associated polycyclic aromatic hydrocarbons and biomarkers. Sci. Total Environ. 287, 121–132. https://doi.org/10.1016/S0048-9697(01)01008-7

Shao, M., Zhang, Y., Zeng, L., Tang, X., Zhang, J., Zhong, L., Wang, B., 2009. Ground-level ozone in the Pearl River Delta and the roles of VOC and NOx in its production. J. Environ. Manage. 90, 512–518. https://doi.org/10.1016/j.jenvman.2007.12.008

Sharma, A., Ojha, N., Pozzer, A., Mar, K.A., Beig, G., Lelieveld, J., Gunthe, S.S., 2017. WRF-Chem simulated surface ozone over south Asia during the pre-monsoon: effects of emission inventories and chemical mechanisms 14393–14413.

Sillman, S., 1999. The relation between ozone, NO and hydrocarbons in urban and polluted rural environments. Atmos. Environ. 33, 1821— 1845.

Sillman, S., 1995. The use of NOy, H_2O_2, and HNO_3 as indicators for ozone-NOx-hydrocarbon sensitivity in urban locations. Jounal Geophys. Res. 100, 14175–14188. https://doi.org/10.1029/94JD02953

Smith, S. J., van Aardenne, J., Klimont, Z., Andres, R., Volke, A., and Delgado Arias, S., 2010. Anthropogenic sulfur dioxide emissions: 18502005, Atmos. Chem. Phys. Discuss., 10,

16111–16151, doi:10.5194/acpd-10-16111-2010

Stathopoulou, E., Mihalakakou, G., Santamouris, M., Bagiorgas, H.S., 2008. On the impact of temperature on tropospheric Ozone mixing ratio levels in urban environments. J. Earth Syst. Sci. 117, 227–236. https://doi.org/10.1007/s12040-008-0027-9

Sun, W., Shao, M., Granier, C., Liu, Y., Ye, C.S., Zheng, J.Y., 2018. Long-Term Trends of Anthropogenic SO2, NOx, CO, and NMVOCs Emissions in China. Earth's Future. 6, 1112–1133. https://doi.org/10.1029/2018EF000822

Tessum, C.W., Hill, J.D., Marshall, J.D., 2015. air quality simulation: performance evaluation. Geosci. Model Dev. 8, 957–973. https://doi.org/10.5194/gmd-8-957-2015

Thompson, G., Field, P.R., Rasmussen, R.M., Hall, W.D., 2008. Explicit Forecasts of Winter Precipitation Using an Improved Bulk Microphysics Scheme. Part II: Implementation of a New Snow Parameterization. Mon. Weather Rev. 136, 5095–5115. https://doi.org/10.1175/2008MWR2387.1

Tokarek, T.W., Brownsey, D.K., Jordan, N., Garner, N.M., Ye, C.Z., Assad, F. V, Schiller, C.L., Mason, R.H., Vingarzan, R., Osthoff, H.D., Brownsey, D.K., Jordan, N., Garner, N.M., Ye, C.Z., 2017. Biogenic Emissions and Nocturnal Ozone Depletion Events at the Amphitrite Point Observatory on Vancouver Island Biogenic Emissions and Nocturnal Ozone Depletion Events at the Amphitrite Point Observatory on Vancouver Island. Atmosphere-Ocean 55, 121–132. https://doi.org/10.1080/07055900.2017.1306687

Uttamang, P., Aneja, V., Hanna, A., 2018. Assessment of gaseous criteria pollutants in the Bangkok Metropolitan. Atmos. Chem. Phys. 12581–12593.

Wang, S., Hao, J., 2012. Air quality management in China: Issues, challenges, and options. J. Environ. Sci. 24, 2–13. https://doi.org/10.1016/S1001-0742(11)60724-9

Wang, S.X., Xing, J., Zhao, B., Jang, C., Hao, J., 2014a. Effectiveness of national air pollution control policies on the air quality in metropolitan areas of China. J. Environ. Sci. (China) 26, 13–22. https://doi.org/10.1016/S1001-0742(13)60381-2

Wang, S.X., Zhao, B., Cai, S.Y., Klimont, Z., Nielsen, C.P., Morikawa, T., Woo, J.H., Kim, Y., Fu, X., Xu, J.Y., Hao, J.M., He, K.B., 2014b. Emission trends and mitigation options for air pollutants in East Asia. Atmos. Chem. Phys. 14, 6571–6603. https://doi.org/10.5194/acp-14-6571-2014

Wałaszek, K., Kryza, M., Werner, M. J, 2018. The role of precursor emissions on ground level ozone mixing ratio during summer season in Poland. Atmos Chem. 75(2), 181–204. https://doi.org/10.1007/s10874-017-9371-y

Xue, L.K., Wang, T., Gao, J., Ding, A.J., Zhou, X.H., Blake, D.R., Wang, X.F., Saunders, S.M., Fan, S.J., Zuo, H.C., Zhang, Q.Z., Wang, W.X., 2014. Ground-level ozone in four Chinese cities: Precursors, regional transport and heterogeneous processes. Atmos. Chem. Phys. 14, 13175–13188. https://doi.org/10.5194/acp-14-13175-2014

Yahya, K., Campbell, P., Zhang, Y., 2017. Decadal application of WRF/chem for regional air

826 quality and climate modeling over the U.S. under the representative mixing ratio pathways
827 scenarios. Part 2: Current vs. future simulations. Atmos. Environ. 152, 584–604.
828 https://doi.org/nttp://dx.doi.org/10.1016/j.atmosenv.2016.12.028

829 Yahya, K., Zhang, Y., Vukovich, J.M., 2014. Real-time air quality forecasting over the
830 southeastern United States using WRF/Chem-MADRID: Multiple-year assessment and
831 sensitivity studies. Atmos. Environ. 92, 318–338.
832 https://doi.org/10.1016/j.atmosenv.2014.04.024

833 Yang, J., Kang, S., Ji, Z., 2018. Sensitivity Analysis of Chemical Mechanisms in the WRF-Chem
834 Model in Reconstructing Aerosol Mixing ratios and Optical Properties in the Tibetan
835 Plateau. Aerosol Air Qual. Res. 18, 505–521. https://doi.org/10.4209/aaqr.2017.05.0156

836 Yerramilli, A., Challa, V.S., Dodla, V.B.R., Dasari, H.P., Young, J.H., Patrick, C., Baham, J.M.,
837 Hughes, R.L., Hardy, M.G., Swanier, S.J., 2010. Simulation of Surface Ozone Pollution in
838 the Central Gulf Coast Region Using WRF/Chem Model: Sensitivity to PBL and Land
839 Surface Physics. Adv. Meteorol. 2010, 1–24. https://doi.org/10.1155/2011/464753

840 Žabkar, R., Koračin, D., Rakovec, J., 2013. A WRF/Chem sensitivity study using ensemble
841 modelling for a high ozone episode in Slovenia and the Northern Adriatic area. Atmos.
842 Environ. 77, 990–1004. https://doi.org/10.1016/j.atmosenv.2013.05.065

843 Zhang, S., Wu, Y., Liu, H., Huang, R., Un, P., Zhou, Y., Fu, L., Hao, J., 2014. Real-world fuel
844 consumption and CO_2 (carbon dioxide) emissions by driving conditions for light-duty
845 passenger vehicles in China. Energy 69, 247–257.
846 https://doi.org/10.1016/j.energy.2014.02.103

847 Zhang, S., Wu, Y., Zhao, B., Wu, X., Shu, J., Hao, J., 2017. City-specific vehicle emission
848 control strategies to achieve stringent emission reduction targets in China's Yangtze River
849 Delta region. J. Environ. Sci. (China) 51, 75–87. https://doi.org/10.1016/j.jes.2016.06.038

850 Zhang, Y., Wen, X.Y., Wang, K., Vijayaraghavan, K., Jacobson, M.Z., 2009. Probing into
851 regional O_3 and particulate matter pollution in the United States: 2. An examination of
852 formation mechanisms through a process analysis technique and sensitivity study. J.
853 Geophys. Res. Atmos. 114, 1–31. https://doi.org/10.1029/2009JDO11900

854 Zimmermann, J., Poppe, D., 1996. A supplement for the RADM2 chemical mechanism: The
855 photooxidation of isoprene. Atmos. Environ. 30, 1255–1269. https://doi.org/10.1016/1352-
856 2310(95)00417-3

857

Table 1. WRF-Chem physical and chemical options used in this study.

Option		Selection
Physics		
	Microphysics	Thompson
	Cumulus parameterization	Grell-Freitas (only domain 1 and 2)
	Long wave radiation	A new version of Rapid Radiative Transfer Model (RRTMG)
	Short wave radiation	RRTMG
	Planetary boundary layer	Yonsei University
	Surface layer	MM5 similarity
	Land surface	Noah Land-Surface model
Chemistry		
	Chemical mechanism	RADM2-MADE/SORGAM
	Photolysis	Madronich F-TUV photolysis
	Dry deposition of gas/aerosol species	On
	Subgrid convective wet scavenging and aqueous chemistry	On (only domain 1 and 2)
	Vertical turbulent mixing	On (only domain 1 and 2)
	Aerosol effect in radiation	On

Table 2. Summarizes baseline simulation and sensitivity simulations.

Simulations	Adjusted China's emissions		Note
	NO_x	VOC	
Baseline	No	No	
Sensitivity			
- Strategy 1 (S1)	10 % reduction	No	The national reduction target during China's 12th FYP (Wang et al., 2014a)
- Strategy 2 (S2)	20 % reduction	No	To examine the responses of O_3 and its precursors in the BMR due to different China's NO_x emission reductions.
- Strategy 3 (S3)	40 % reduction	No	
- Strategy 4 (S4)	40 % reduction	40 % reduction	To investigate implications for incorporating VOC emission reduction. (Wang and Hao, 2012)

Table 3. Summary of the averaged statistics for January to March 2010.

Variable	Statistics	Station ID															Overall
		3T	10T	11T	14T	15T	19T	21T	22T	24T	26T	27T	34T	41T	52T	60T	61T	
T	$\overline{Obs}$	29.59	29.39	29.71	28.93	30.12	28.71	28.12	29.14	28.97	28.91	29.24	30.87	30.61	29.43	27.98	30.09	29.36
(°C)	$\overline{Sim}$	26.74	25.93	26.18	26.27	26.72	26.9	27.25	26.27	27.07	26.59	26.94	26	26.75	26.47	26.58	25.99	26.54
	r	0.78	0.86	0.85	0.77	0.78	0.8	0.9	0.89	0.89	0.89	0.80	0.56	0.83	0.84	0.87	0.85	0.82
	MB	-2.85	-3.47	-3.53	-2.67	-3.39	-1.81	-0.88	-2.87	-1.91	-2.32	-2.30	-4.87	-3.86	-2.97	-1.40	-4.10	-2.83
	RMSE	4.21	4.6	4.61	4.1	4.72	3.58	2.1	3.87	2.74	3.02	3.92	6.00	4.59	4.28	2.77	5.29	4.03
	NMB	-9.62	-11.79	-11.91	-9.21	-11.27	-6.3	-3.13	-9.85	-6.59	-8.01	-7.86	-15.77	-12.61	-10.08	-5.01	-13.63	-9.54
WS	$\overline{Obs}$	2.12	2.01	1.02	1.57	1.14	2.53	1.5	1.23	1.78	2	2.06	1.93	1.09	1.71	2.03	1.64	1.71
(ms^{-1})	$\overline{Sim}$	3.29	3.03	2.73	3.04	3.37	3.19	3.25	3.26	4.15	3.08	3.23	4.09	4.17	3.04	3.26	3.47	3.35
	r	-0.03	0.04	0.01	0.16	0.13	0.01	0.26	0.35	0.32	0.48	0.15	0.04	0.23	0.12	0.24	0.07	0.16
	MB	1.17	1.02	0.49	1.46	2.22	0.66	1.25	2.03	2.38	1.13	1.17	2.17	3.08	1.33	1.23	1.82	1.54
	RMSE	2.19	1.84	1.17	2.05	2.75	2.03	2.13	2.45	3.34	1.75	2.01	2.91	3.65	20.1	3	2.53	3.49
	NMB	55.39	50.76	197.41	92.92	194.66	26.25	121.9	165.03	133.57	57.74	56.91	112.11	282.4	77.93	60.35	110.85	112.26
RH	$\overline{Obs}$	73.11	67.08	65.19		69.81	75.46	66.38	74.46	68.19	68.93	72.4	72.53	62.12	60.14	74.54		69.31
(%)	$\overline{Sim}$	61.99	65.97	65.6		62.49	59.21	61.48	64.63	60.47	64.31	61.08	59.89	64	63.67	59.71		62.46
	r	0.68	0.77	0.74		0.68	0.64	0.71	0.78	0.74	0.79	0.6	0.59	0.65	0.67	0.71		0.70
	MB	-11.11	-1.11	0.41	N/A	-7.32	-16.25	-4.94	-9.83	-7.70	-4.61	-11.31	-12.63	1.88	3.53	-14.82	N/A	-6.84
	RMSE	17.32	12.61	12.7		15.29	21.26	14.61	16.27	14.28	11.68	18.06	18.96	15.25	14.35	20.08		15.91
	NMB	19.61	-1.65	0.63		-10.49	-21.53	-7.44	-13.2	-11.3	-6.69	-15.65	-17.41	3.03	5.87	-19.88		-6.86
P	$\overline{Obs}$	758.29	757.02	758.94	757.29	758.73	757.48	756.13	758.64	753.61	759.66	759.60	762.43	747.32	759.73	764.33	760.20	758.09
(hPa)	$\overline{Sim}$	759.09	759.23	759.39	758.92	758.97	754.70	759.20	759.34	756.54	757.82	758.16	733.64	757.23	759.20	755.15	759.23	756.61
	r	0.76	0.83	0.80	0.78	0.78	0.64	0.81	0.74	0.78	0.83	0.77	0.79	0.53	0.81	0.65	0.76	0.75
	MB	0.79	2.22	0.45	1.63	0.24	-2.78	3.07	0.70	2.93	-1.84	-1.44	-28.78	9.91	-0.53	-9.18	-0.97	-1.47
	RMSE	1.63	2.53	1.37	2.47	1.36	3.27	3.32	1.63	3.23	2.16	1.98	28.81	10.11	1.33	9.83	1.65	4.79
	NMB	0.11	0.29	0.06	0.22	0.03	-0.37	0.41	0.09	0.39	-0.24	-0.19	-3.77	1.33	-0.07	-1.20	-0.13	-0.19
Max	$\overline{Obs}$	30.1	25.20	16.27	20.45	20.51	26.53	10.88	22.68	21.53	29.68	33.85	28.54	33.86	30.43	33.56	28.62	23.68*
8-h O_3	$\overline{Sim}$	15.85	19.25	19.41	17.26	17.28	13.61	18.89	14.32	20.01	5.62	16.05	31.22	48.90	26.75	16.68	31.03	22.63*
(ppb)	r	0.42	0.38	0.16	0.26	0.26	-0.03	0.42	0.56	0.58	-0.27	-0.02	-0.09	0.30	0.44	0.10	0.53	0.39*
	MB	-14.25	-5.95	3.14	-3.19	-3.23	-12.92	3.07	-8.37	-1.53	-24.06	-17.80	2.68	15.04	-3.68	-16.88	2.40	-1.96*
	RMSE	18.31	14.91	17.44	16.88	16.88	19.87	7.46	12.92	12.44	27.56	56.68	23.75	25.13	17.55	22.07	19.18	17.16*
	MNBE	-46.98	-18.87	38.33	-5.77	-5.98	-29.77	39.13	-34.45	-1.88	-74.48	-48.07	22.08	49.66	-13.04	-47.77	6.81	-3.22*

Note: *data from 19T, 26T, 27T, 34T and 60T are excluded.

Table 4. Summarized delta O_3, NO_x, CO, VOC, PAN, HNO_3 and O_x in the regional scale (d01) due to the China's emission reductions during January to March 2010.

Species (ppb)	January				February				March			
	S1	S2	S3	S4	S1	S2	S3	S4	S1	S2	S3	S4
O_3	0.35±0.54 (0.9%)	0.72±.78 (1.9%)	1.53±1.49 (4.1%)	1.34±1.39 (3.5%)	0.35±0.69 (0.9%)	0.62±1.07 (1.5%)	1.27±2.07 (3.2%)	1.11±1.87 (2.8%)	0.30±0.80 (0.7%)	0.55±1.06 (1.3%)	1.17±2.0 (2.7%)	1.01±1.80 (2.3%)
NO_x	-5.41±10.76 (-10.4%)	-10.98±20.57 (-21.1%)	-20.53±38.82 (-39.4%)	-20.45±38.76 (-39.2%)	-4.15±9.04 (-10.9%)	-7.94±16.73 (-20.8%)	-14.91±31.33 (-39.1%)	-14.84±31.19 (-38.9%)	-2.41±8.41 (-9.7%)	-4.64±12.22 (-18.6%)	-9.34±20.79 (-37.5%)	-9.24±20.79 (-37.1%)
CO	-0.10±4.58 (-0.1%)	-0.31±3.65 (-0.2%)	-0.30±3.99 (-0.2%)	-0.46±3.96 (-0.2%)	-0.16±3.96 (-0.1%)	-0.13±3.90 (-0.1%)	-0.25±4.03 (-0.1%)	-0.39±3.86 (-0.2%)	0.03±8.69 (0.0%)	0.03±9.42 (0.0%)	-0.16±9.07 (-0.1%)	-0.17±9.42 (-0.1%)
VOC	0.01±0.40 (0.1%)	-0.03±0.29 (-0.3%)	-0.05±0.35 (-0.5%)	-1.06±1.81 (-11.6%)	0.01±0.50 (0.1%)	0.0±0.53 (0.0%)	-0.03±0.55 (-0.3%)	-0.80±1.64 (-9.2%)	0.07±1.26 (0.7%)	0.06±1.32 (0.8%)	0.02±1.27 (0.2%)	-0.55±1.82 (-6.5%)
PAN	0.01±0.02 (1.4%)	0.01±0.02 (2.7%)	0.03±0.04 (6.5%)	0.02±0.03 (4.0%)	0.01±0.03 (0.9%)	0.01±0.04 (1.9%)	0.02±0.05 (4.3%)	0.01±0.04 (2.3%)	0.007±0.05 (1.2%)	0.01±0.05 (2.1%)	0.03±0.07 (4.7%)	0.02±0.06 (2.9%)
HNO_3	-0.07±0.18 (-2.2%)	-0.18±0.24 (-5.5%)	-0.42±0.47 (-13.1%)	-0.46±0.48 (-14.0%)	-0.11±0.21 (-3.0%)	-0.22±0.32 (-6.3%)	-0.49±0.64 (-13.9%)	-0.50±0.65 (-14.3%)	-0.09±0.18 (-3.0%)	-0.16±0.23 (-5.6%)	-0.35±0.43 (-12.3%)	-0.36±0.45 (-12.4%)
O_x	-1.90±3.98 (-2.8%)	-3.80±7.57 (-5.6%)	-7.49±15.15 (-11.1%)	-7.76±15.20 (-11.5%)	-1.33±2.93 (-2.1%)	-2.67±5.63 (-4.2%)	-5.38±11.43 (-8.4%)	-5.59±11.57 (-8.8%)	-0.93±2.21 (-1.5%)	-1.82±4.03 (-3.0%)	-3.80±8.16 (-6.3%)	-3.98±8.33 (-6.6%)

Table 5. Summarized delta O_3, NO_x, CO, VOC, PAN, HNO_3 and O_x on the local scale (d03) due to the China's emission reduction strategies during January to March 2010.

Species (ppb)	January				February				March			
	S1	S2	S3	S4	S1	S2	S3	S4	S1	S2	S3	S4
O_3	0.53±1.66 (1.5%)	1.20±1.57 (3.5%)	2.15±2.03 (6.2%)	1.95±1.96 (5.6%)	1.32±3.10 (2.2%)	1.64±3.09 (2.7%)	2.98±3.42 (5.0%)	2.55±3.18 (4.2%)	-0.34±5.78 (-0.4%)	0.16±6.39 (0.2%)	0.90±6.46 (1.1%)	0.70±44.47 (1.2%)
NO_x	2.60±33.73 (0.6%)	-10.62±26.52 (-2.5%)	-18.40±30.20 (-4.4%)	-18.76±30.66 (-4.4%)	-2.93±43.36 (-0.8%)	-3.26±41.42 (-0.9%)	-5.33±42.45 (-1.5%)	-6.72±40.68 (-1.9%)	22.98±76.75 (7.6%)	28.15±82.10 (9.0%)	24.44±78.90 (7.8%)	22.02±406.89 (3.7%)
CO	10.59±43.58 (1.5%)	-0.01±33.85 (0.0%)	3.38±38.38 (0.5%)	1.80±39.58 (0.3%)	-1.03±56.70 (-0.2%)	1.46±54.35 (0.2%)	3.94±55.85 (0.6%)	1.12±53.43 (0.2%)	36.92±100.96 (6.0%)	39.81±109.17 (6.5%)	36.41±105.73 (5.9%)	39.47±108.83 (6.4%)
VOC	1.32±5.03 (1.2%)	0.32±4.20 (0.3%)	1.28±4.59 (1.2%)	-0.55±4.56 (-0.5%)	0.13±8.09 (0.1%)	0.34±8.21 (0.3%)	0.81±8.37 (0.7%)	0.12±7.97 (0.1%)	4.44±15.90 (3.4%)	6.22±15.96 (4.7%)	5.25±15.66 (4.0%)	-4.56±113.39 (-2.3%)
PAN	0.01±0.17 (1.1%)	0.02±0.16 (2.6%)	0.05±0.20 (5.2%)	0.04±0.18 (4.5%)	0.04±0.38 (2.2%)	0.06±0.37 (2.8%)	0.12±0.39 (5.9%)	0.09±0.36 (4.7%)	0.06±0.70 (1.7%)	0.09±0.72 (2.6%)	0.09±0.71 (2.5%)	0.09±0.70 (2.6%)
HNO_3	0.03±0.26 (0.62%)	0.06±0.24 (1.4%)	0.14±0.40 (3.0%)	-0.04±0.33 (-0.9%)	0.06±0.70 (0.5%)	-0.16±0.69 (-1.4%)	-0.38±0.77 (-3.3%)	-0.45±0.78 (-3.9%)	-0.39±0.95 (-2.9%)	-0.49±0.97 (-3.7%)	-0.49±0.97 (-3.7%)	-0.51±0.95 (-3.8%)

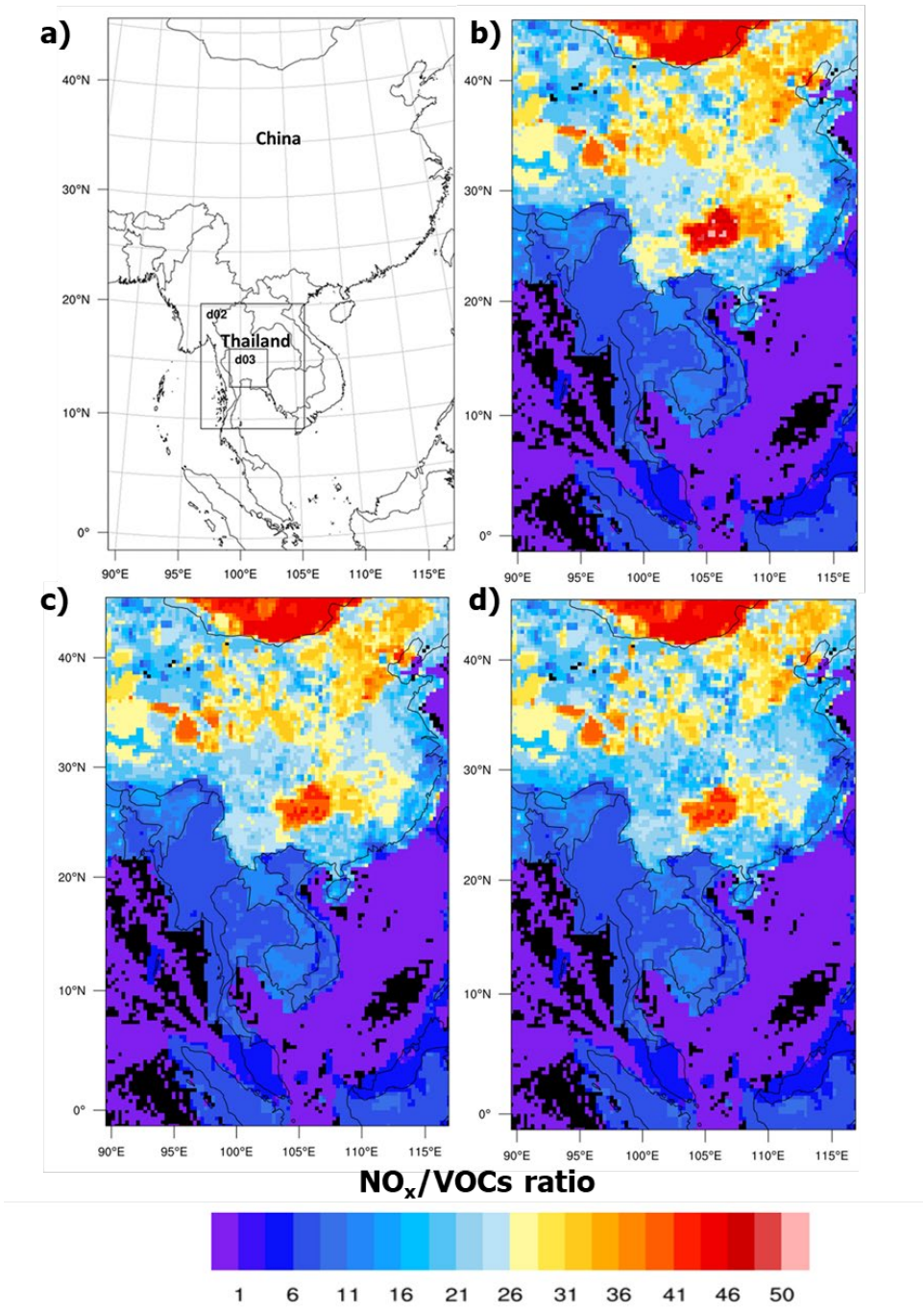

Figure 1. a) A triple-nested domain, including outermost domain (d01), the second domain (d02) and the innermost domain (d03) with 36-, 12- and 4-km horizontal resolutions, respectively; b) to d) NO_x/VOCs emission during January, February and March, respectively.

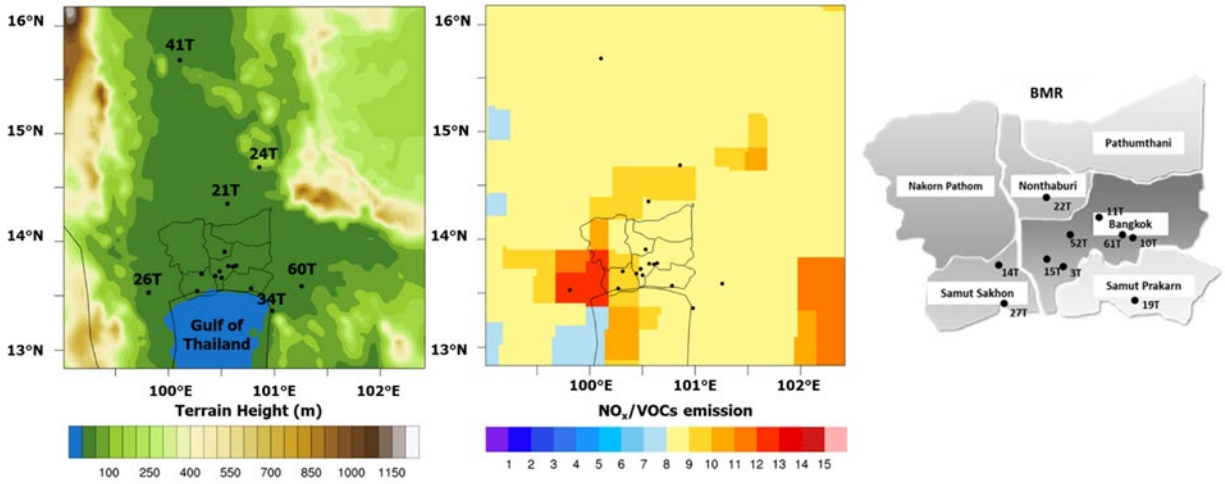

Figure 2. Terrain height in d03, NO_x/VOCs emission in d03 and the location of 16 monitoring stations which six stations located outside of the BMR and 10 stations located inside of the BMR for the model evaluation.

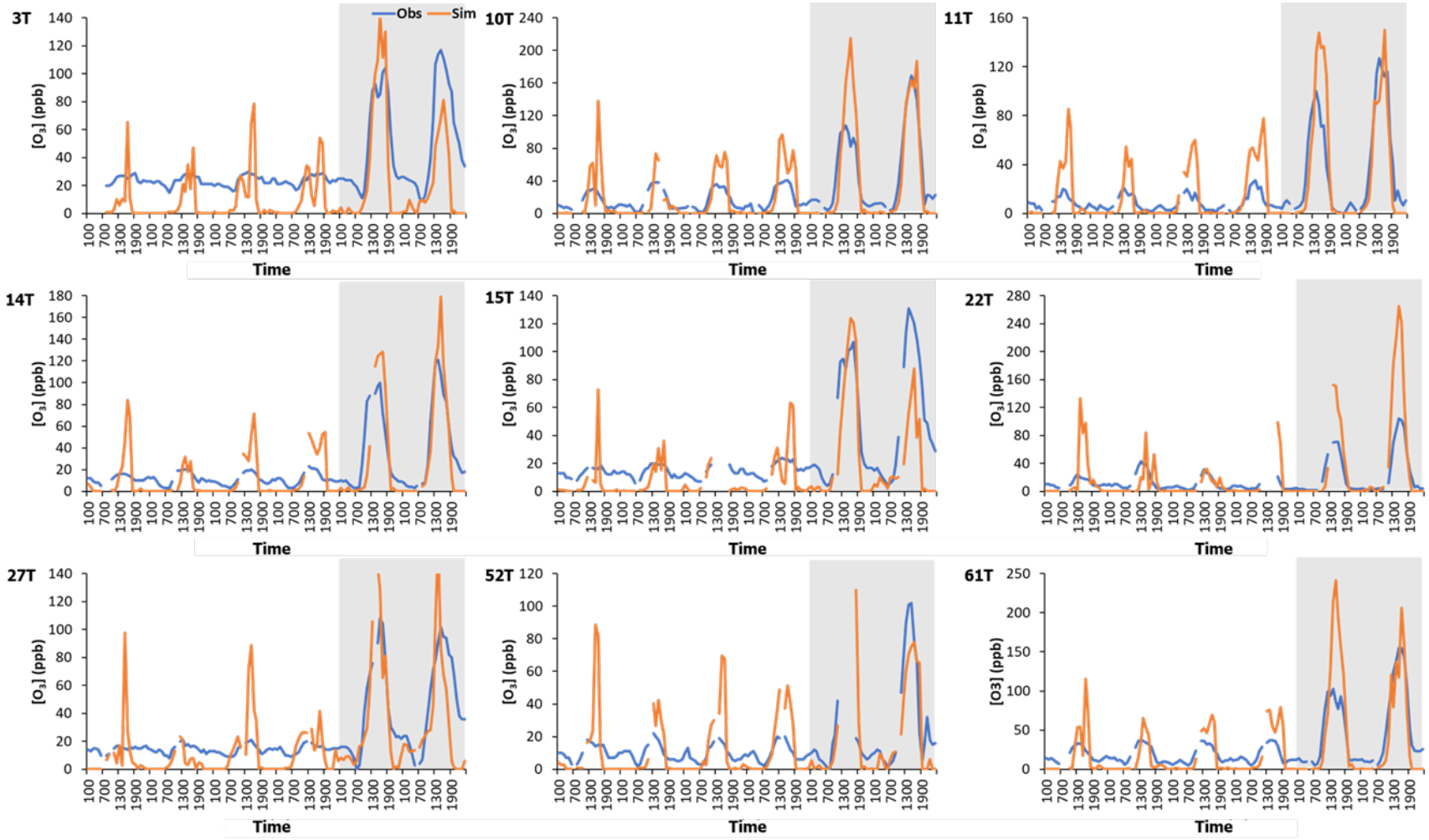

Figure 3. Temporal variations of hourly observed (blue) and simulated (orange) O_3 concentrations during 1 to 6 March 2010 at nine monitoring stations. The shaded areas refer to the O_3 episode. Simulated hourly O_3 concentrations are not presented when observations are missing.

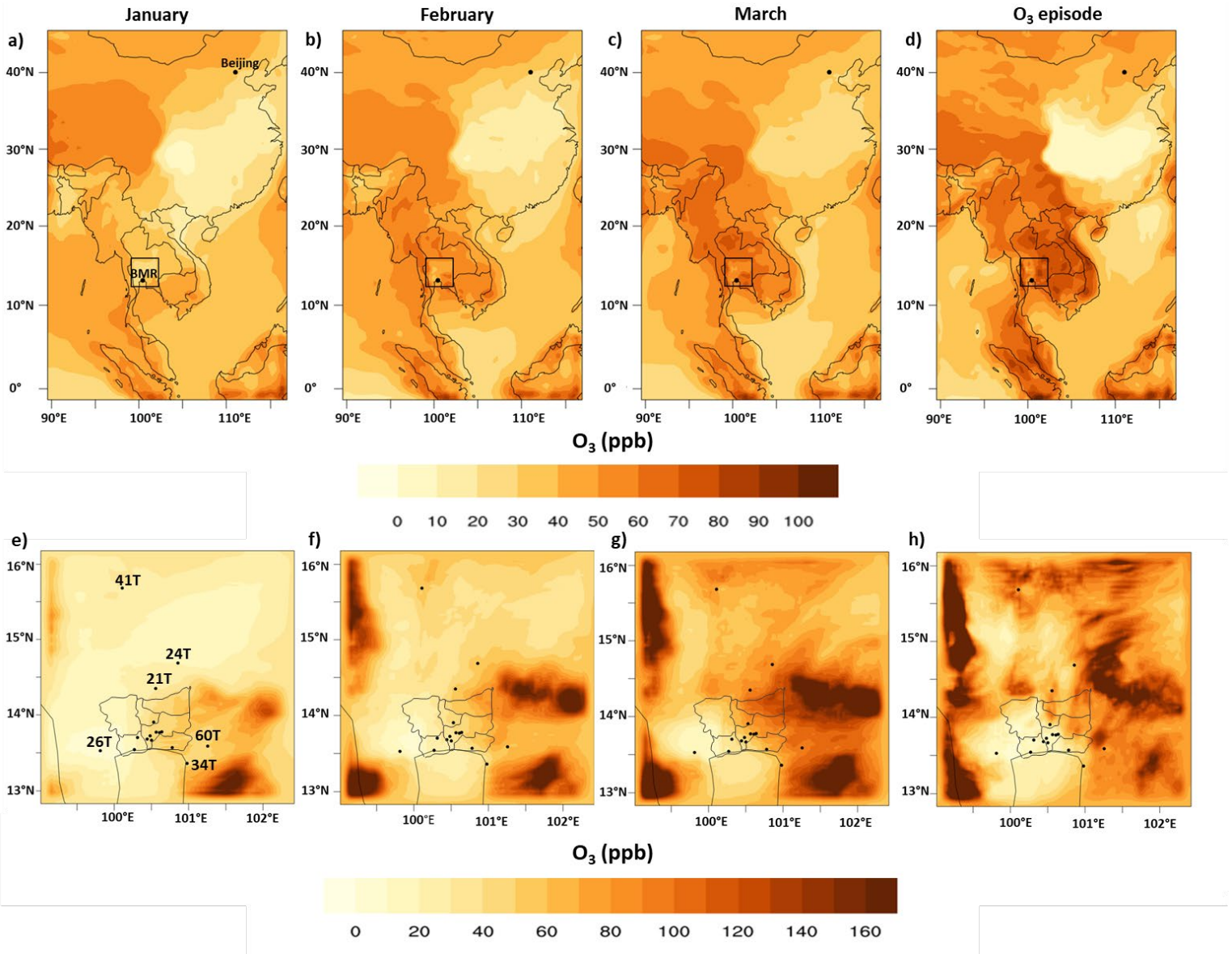

Figure 4. Spatial distributions of average O_3 from the baseline simulation in d01 and in d03 for the months of a) and e) January, b) and f) February, c) and g) March, and d) and h) the episodic O_3 event period. Small boxes indicate the boundary of d03 compared with d01.

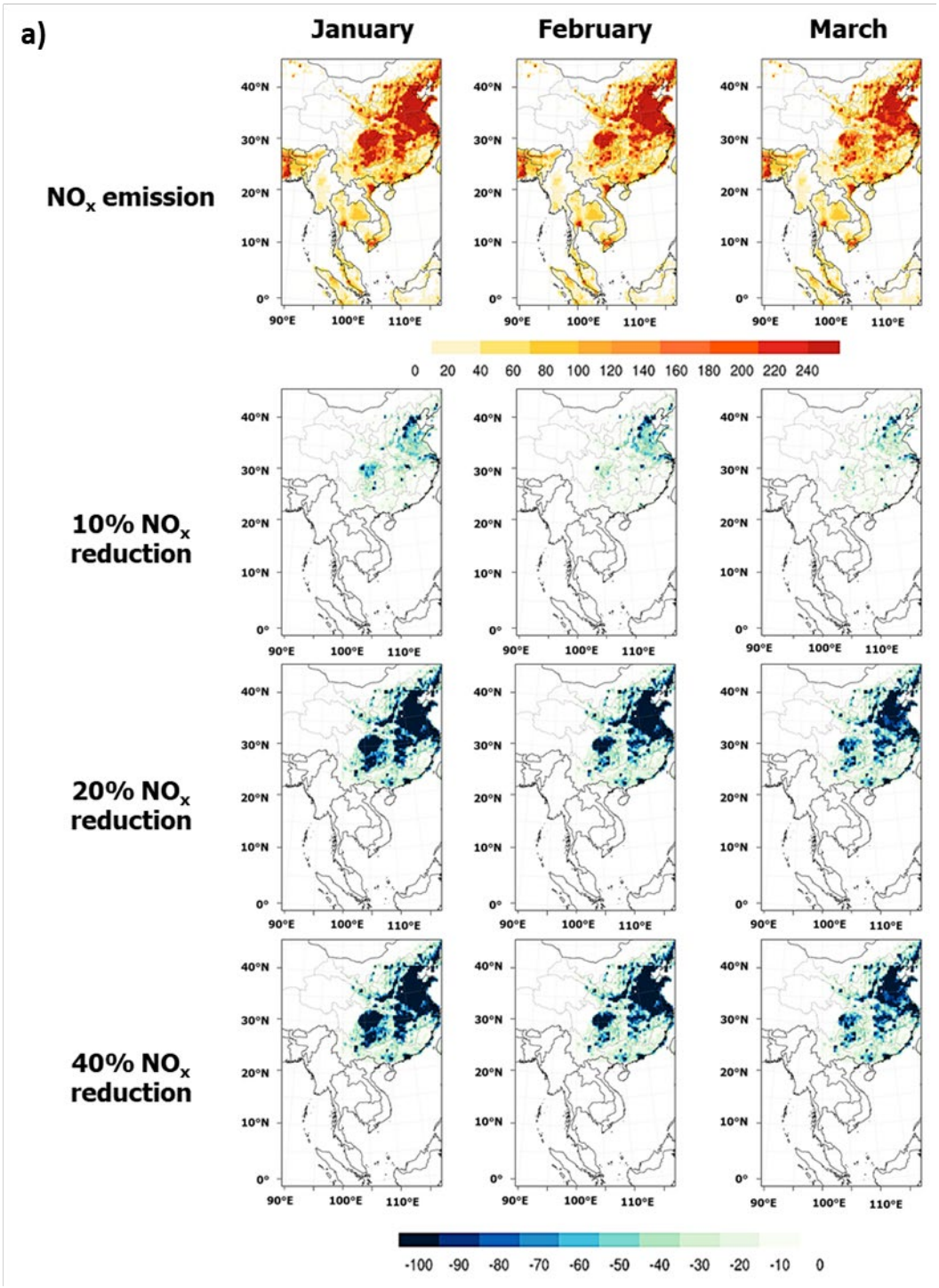
a)
January
February
March
NOx emission
10% NOx reduction
20% NOx reduction
40% NOx reduction
40°N
30°N
20°N
10°N
0°
90°E
100°E
110°E
0 20 40 60 80 100 120 140 160 180 200 220 240
-100 -90 -80 -70 -60 -50 -40 -30 -20 -10 0

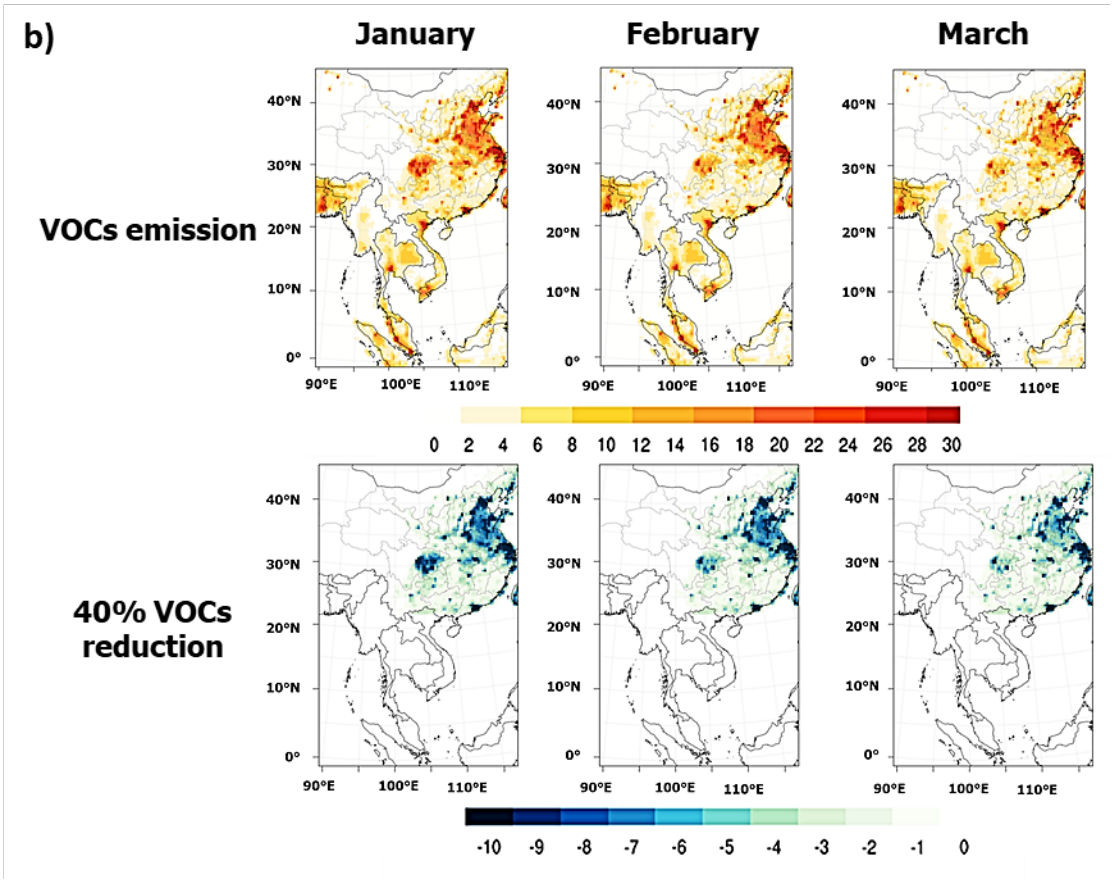

Figure 5. Monthly-average a) NO_x and b) VOC emissions and absolute differences of emissions (sensitivity – baseline) based on S1 to S4 in January to March 2010.

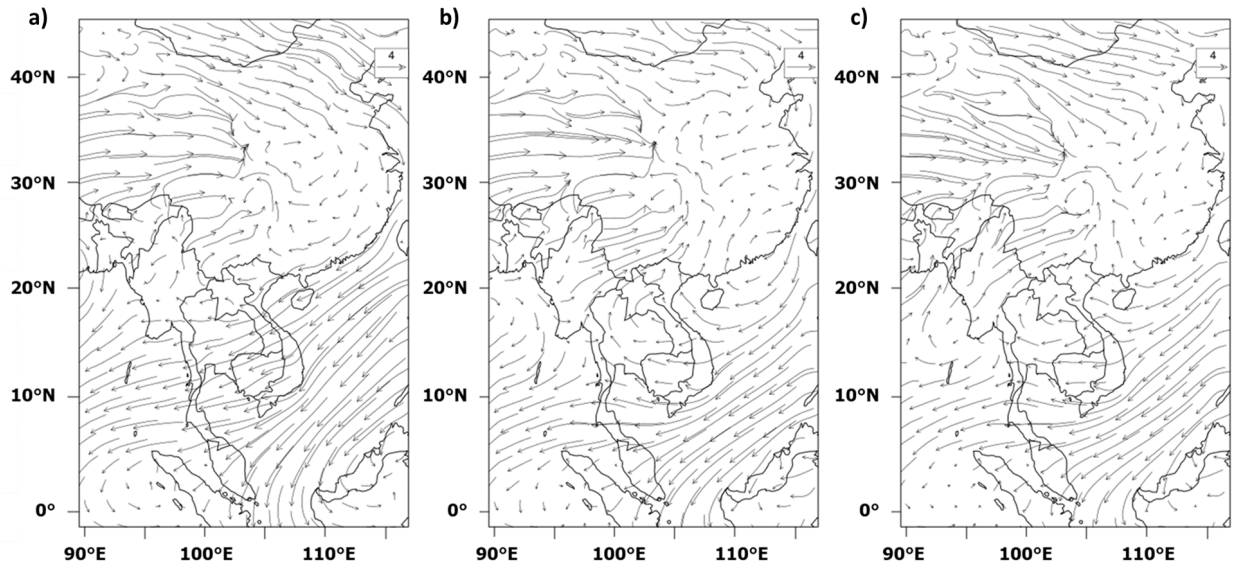

Figure 6. Monthly-average wind field during a) January b) February and c) March 2010 in d01.

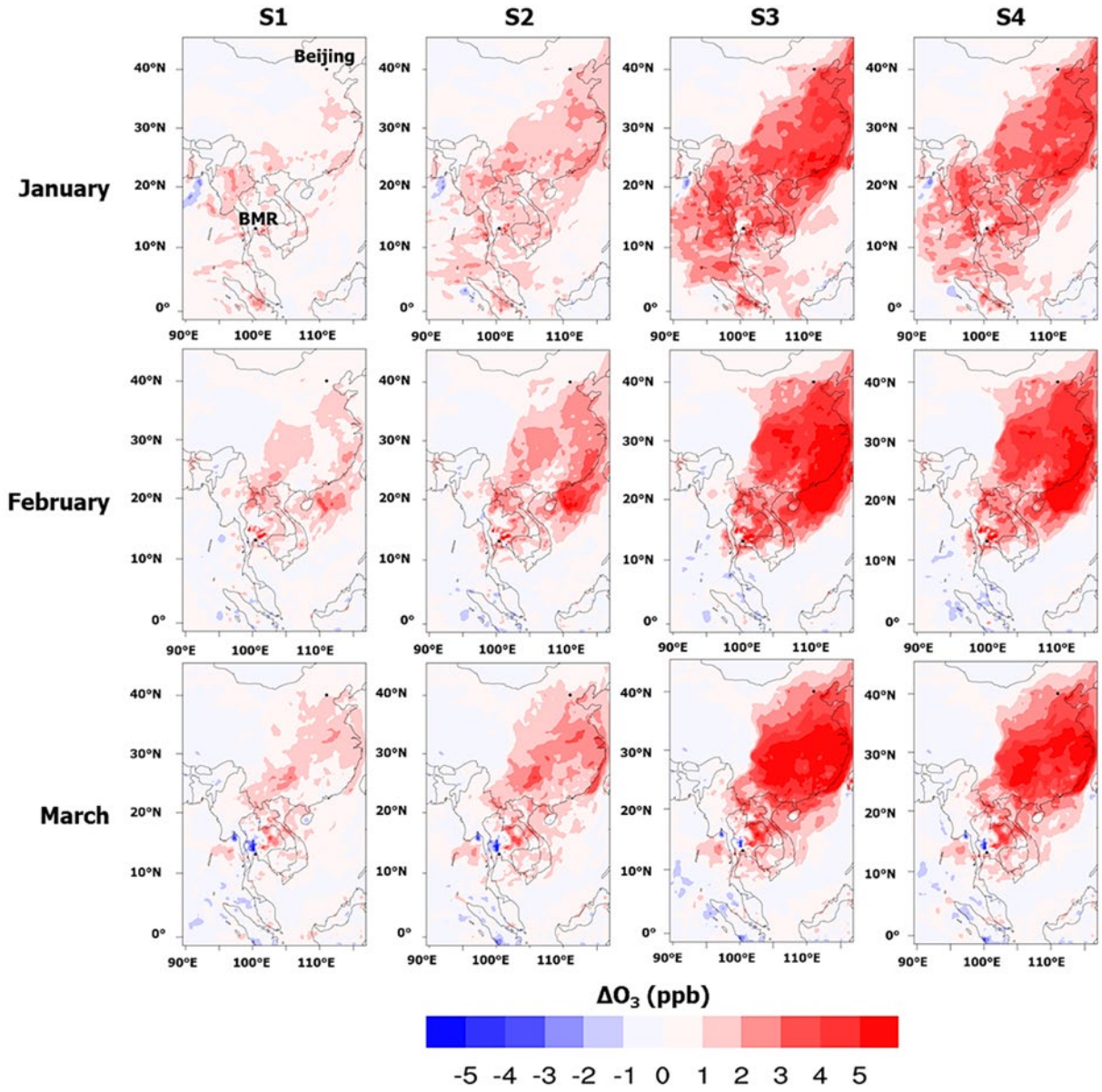

Figure 7. Spatial distributions of monthly-average delta O_3 on the regional scale (d01) due to China's emission reductions during January to March 2010.

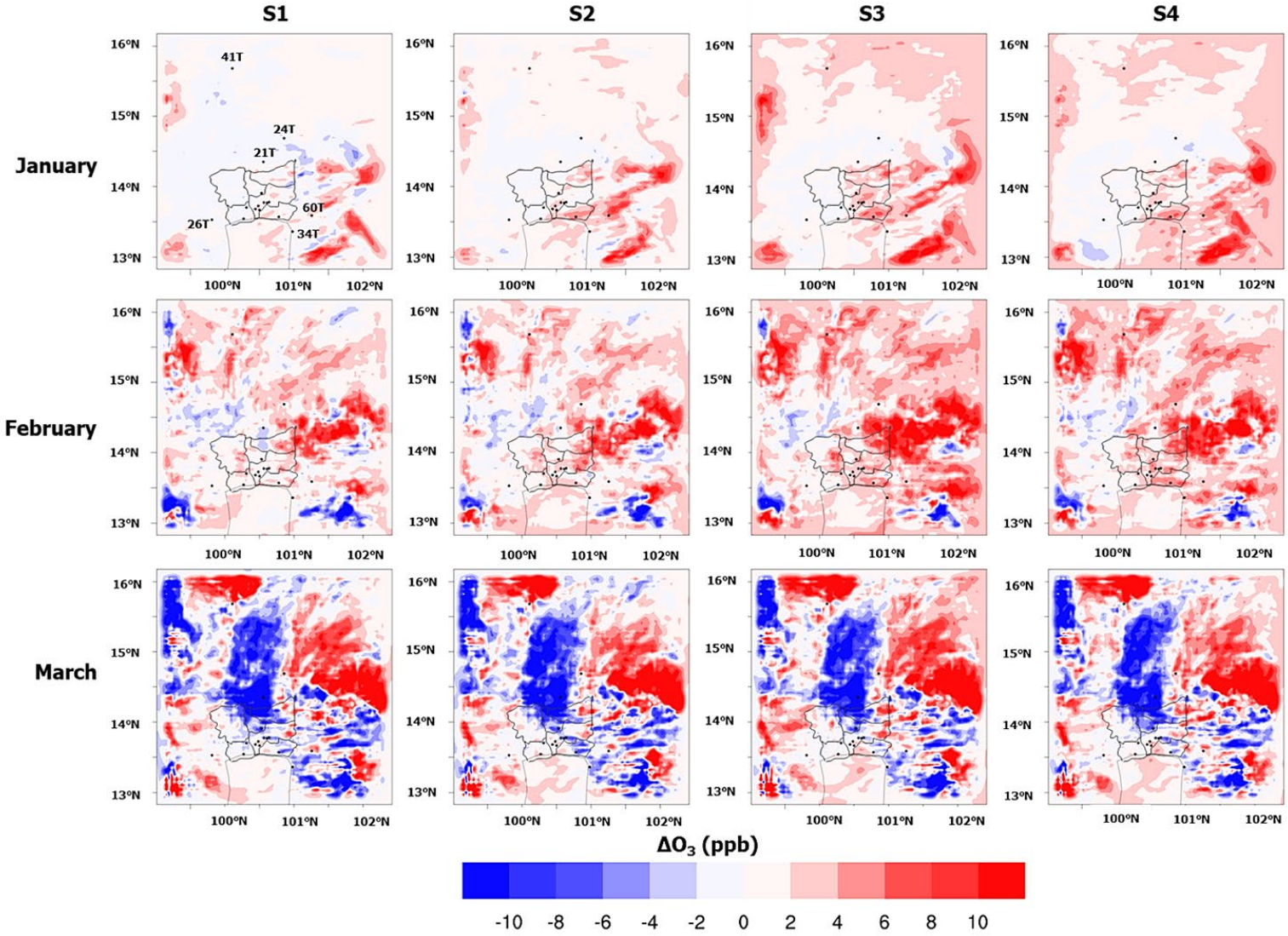

Figure 8. Spatial distribution of monthly-average delta O_3 on the local scale (d03) due to the China's emission reduction strategies during January to March 2010.

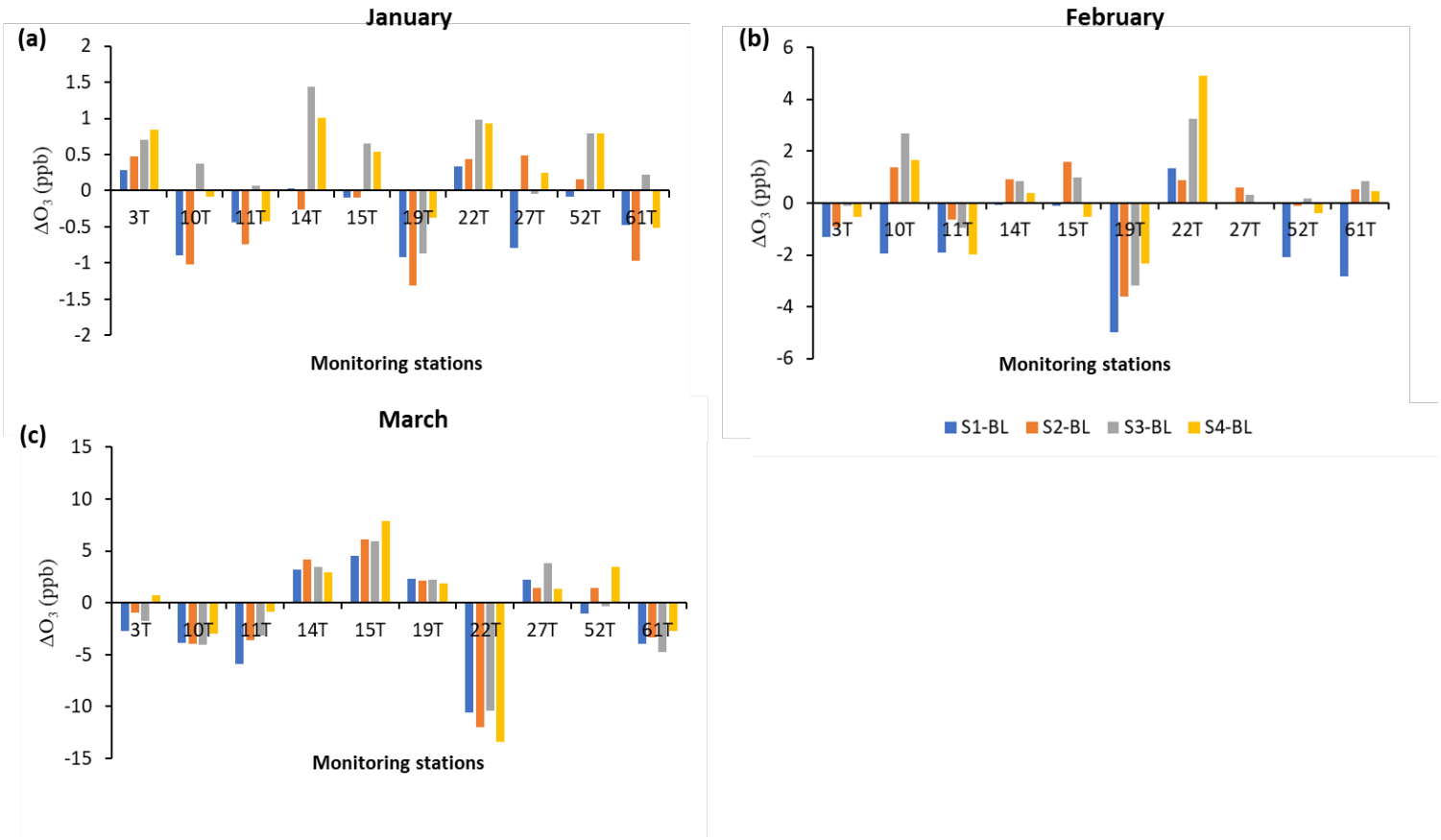

Figure 9. Change of O_3 levels due to China's emission control strategies at 10 monitoring stations in (a) January, (b) February and (c) March 2010 in the BMR. S1-BL, S2-BL, S3-BL and S4-BL refer to the differences between O_3 concentrations simulated from strategy 1, 2, 3 and 4 with baseline simulation, respectively.

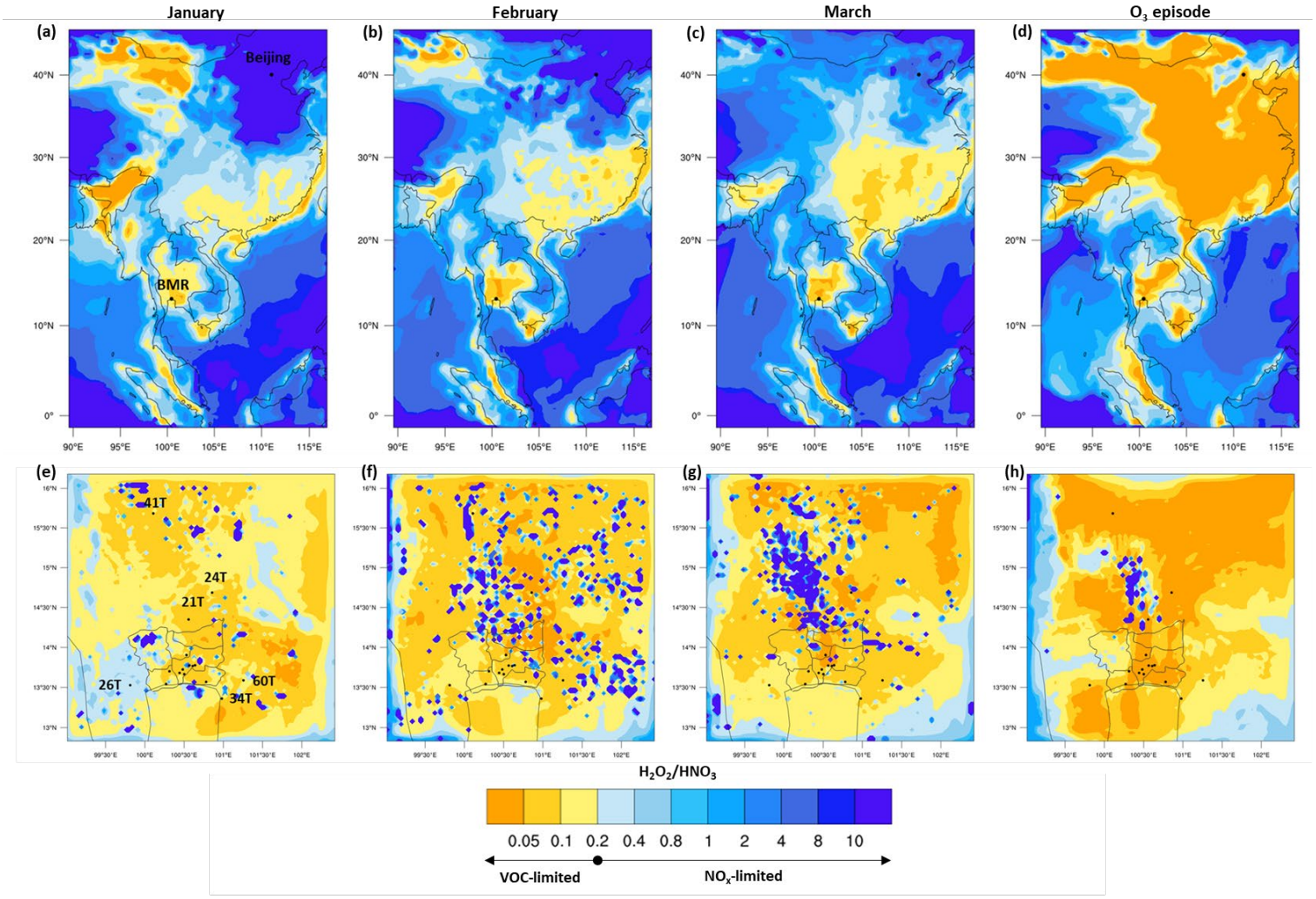

Figure 10. Spatial distributions of monthly-average and episodic-average H_2O_2/HNO_3 from the baseline simulation on the regional (d01) and local scales (d03) during a) and e) January, b) and f) February, c) and g) March and d) and h) the O_3 event 2010, respectively.

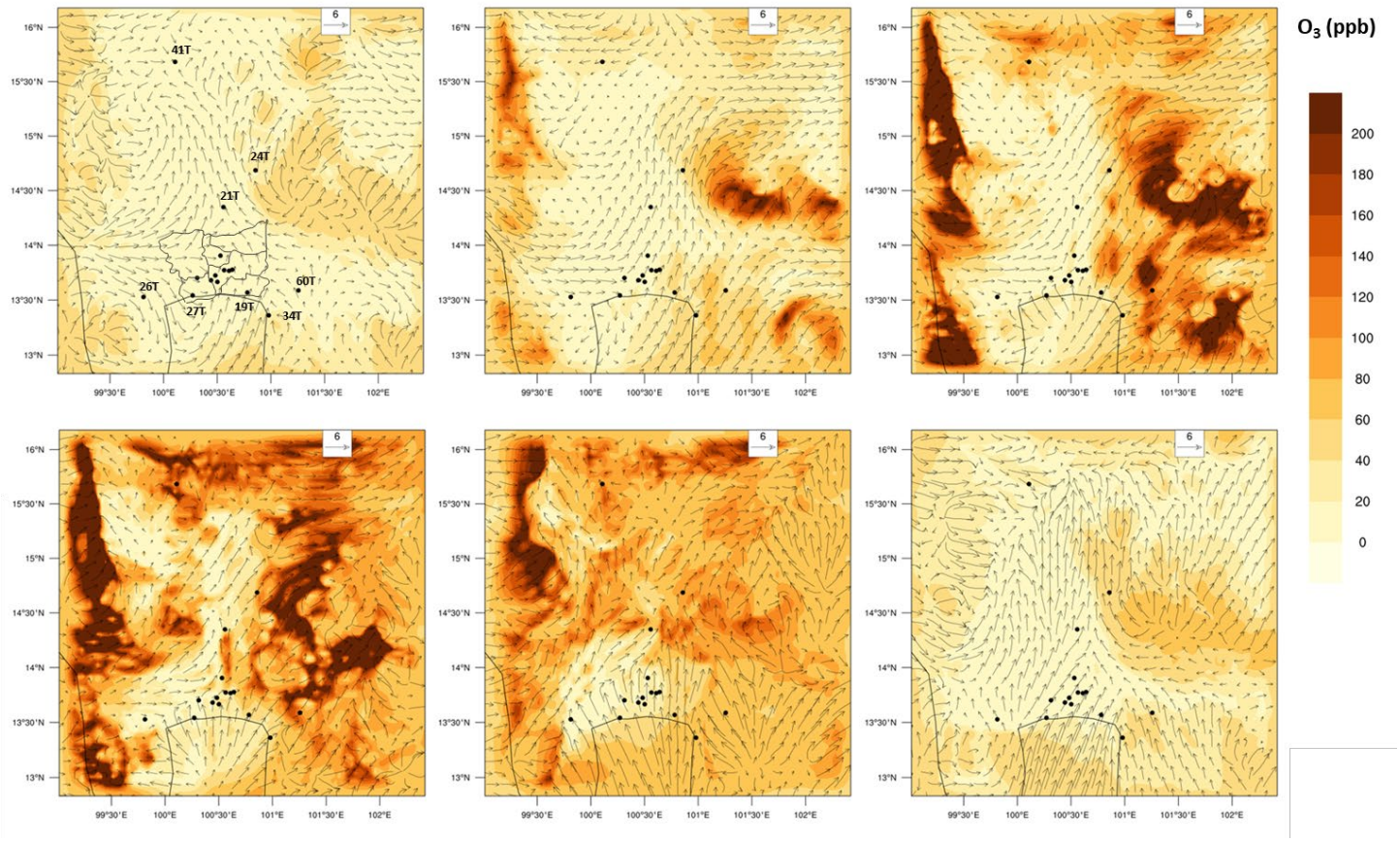

Figure 11. Diurnal cycle of O_3 in the local scale (d03) at (from left-right and top-down) 05:00 LT, 10:00 LT, 12:00 LT, 14:00 LT, 18:00 LT and 23:00 LT of 5 March 2010.